Article

Identification of Novel Dopamine D₂ Receptor Ligands—A Combined In Silico/In Vitro Approach

Lukas Zell, Constanze Lainer, Jakub Kollár, Veronika Temml and Daniela Schuster *

Department of Pharmaceutical and Medicinal Chemistry, Institute of Pharmacy, Paracelsus Medical University, 5020 Salzburg, Austria; lukas.zell@pmu.ac.at (L.Z.); constanze@lainer.co.at (C.L.); jakub.kollar@pmu.ac.at (J.K.); veronika.temml@pmu.ac.at (V.T.)

* Correspondence: daniela.schuster@pmu.ac.at; Tel.: +43-699-14420025

Abstract: Diseases of the central nervous system are an alarming global problem showing an increasing prevalence. Dopamine receptor D_2 (D_2R) has been shown to be involved in central nervous system diseases. While different D_2R-targeting drugs have been approved by the FDA, they all suffer from major drawbacks due to promiscuous receptor activity leading to adverse effects. Increasing the number of potential D_2R-targeting drug candidates bears the possibility of discovering molecules with less severe side-effect profiles. In dire need of novel D_2R ligands for drug development, combined in silico/in vitro approaches have been shown to be efficient strategies. In this study, in silico pharmacophore models were generated utilizing both ligand- and structure-based approaches. Subsequently, different databases were screened for novel D_2R ligands. Selected virtual hits were investigated in vitro, quantifying their binding affinity towards D_2R. This workflow successfully identified six novel D_2R ligands exerting micro- to nanomolar (most active compound $K_I = 4.1$ nM) activities. Thus, the four pharmacophore models showed prospective true-positive hit rates in between 4.5% and 12%. The developed workflow and identified ligands could aid in developing novel drug candidates for D_2R-associated pathologies.

Keywords: dopamine receptor; GPCR; in silico; pharmacophore modelling; virtual screening; in vitro; HTRF

1. Introduction

Diseases of the central nervous system in general show a trend towards an increasing prevalence. Neurodegenerative diseases represent an especially alarming global problem, which is directly linked to the increased life expectancy. The family of G protein-coupled receptors (GPCRs) represents the most important drug targets for currently approved drugs and is still a rich target resource in current drug research [1]. Various subgroups of GPCRs are known to be centrally involved in central nervous system diseases [2]. One of the most prominent members of the GPCR family is the dopamine receptor (DR) family, which is involved in Parkinson's disease, schizophrenia, bipolar disorders, and other pathologies. Throughout the last decades, 65 drugs targeting the DR family have been approved by the US Food and Drug Administration (FDA) [3]. DR-targeting drugs affect their targets with a variety of different modes of action, for example, DR-antagonistic antipsychotics, DR partial agonists used in bipolar disorders and addiction, and antiparkinsonian DR agonists [4–7].

While all DR subtypes are highly interesting, DR D_2 (D_2R) especially has been shown to be involved in all of the conditions listed above. Out of the 65 FDA-approved drugs, 60 also target D_2R [3]. Current therapies of PD, for example, involve D_2R ligands levodopa or apomorphine [8,9]. Amoxapine, aripiprazole, and haloperidol are used in the treatment of depression, psychosis, or schizophrenia [10]. While these drugs are successful in treating the respective conditions, they all suffer from major drawbacks. Dopamine receptor

agonists such as levodopa initially improve motor symptoms in Parkinson's disease patients, reducing so-called off periods. However, levodopa therapy efficacy decreases with time. Moreover, it is problematic in chronic settings due to treatment-induced dyskinesia and other levodopa-induced motor symptoms such as postural abnormalities and speech impairments [11]. Moreover, levodopa treatment involves non-motor side effects such as nausea, depression, insomnia, and gambling addiction [12]. Apomorphine is generally well-tolerated in terms of non-motor symptoms. However, its safety and efficacy suffers from low bioavailability due to intense first-pass metabolism and adverse skin reactions depending on drug administration [8]. These side effects during treatment of Parkinson´s disease with levodopa or apomorphine can lead to a reduction in the quality of life and, subsequently, to discontinuation of the therapy. The use of D_2R antagonists as antipsychotics in several DR-related psychiatric disorders is a standard therapeutic approach. However, these antipsychotics are also tightly associated with adverse side effects such as extrapyramidal syndrome and neuroleptic malignant syndrome [13,14]. The high prevalence of side effects in the treatments targeting D_2R is also due to the promiscuity of the used therapeutics [15]. None of the 60 drugs approved by the FDA are truly selective for D_2R but are also associated with other members of the DR family [3]. Moreover, D_2R-targeting agents also act on closely related receptors from other GPCR families such as different subtypes of the adenosine or serotonin receptor families [16]. The last successful approval of a drug targeting D_2R was levodopa in 2015. Several clinical trials have been discontinued due to insufficient efficacy. Four trials investigating dopamine receptor agonists in Parkinson's disease (PF-06412562, PF-06669571, PF-06649751, and CJH1) are currently ongoing [17]. This illustrates the high demand for novel D_2R-targeting agents.

Drug research regarding GPCR-targeting agents has been driven by the so-called "golden age for GPCR structural biology" in cheminformatics [18]. High-resolution 3D structures with bound ligands provide the means for rational structure-based (SB) drug design. As of today, there are five 3D structures available in the Protein Data Bank (PDB). Three X-ray structures are bound to an antagonist (6cm4 [19] bound to risperidone, 7dfp [20] bound to spiperone, and 6luq [21] bound to haloperidol). Two cryo-EM structures are bound to agonists (6vms [22] and 7jvr [23], both in complex with bromocriptine). They further contribute to understanding the receptor–ligand interaction and the mode of action for D_2R. The most recent entry 7jvr has not been utilized in SB virtual screening yet. While SB approaches are highly valuable, they are limited by the scarcity of available crystal structures considering GPCRs in general and specifically D_2R. Thus, ligand-based (LB) virtual screening approaches present an important complementary approach. They exploit the availability of an ever-growing number of drug-like small molecules offering a spectrum of chemical scaffolds with known biological and pharmacological profiles [24]. This was shown in different studies investigating D_2R agonists. Therefore, the combination of SB and LB virtual screening approaches is recommended to cover a broad chemical space of active compounds in screening campaigns [25–38].

Virtual screening approaches investigating D_2R also greatly benefit from the pioneering work of Floresca and Schentz in describing the orthosteric binding pocket (shown in Figure 1) of the receptor [39]. To enable direct comparisons of different receptor-binding pockets, they relied on the Ballesteros–Weinstein numbering [40]. Applying this approach (e.g., X.50), amino acid positions are annotated based on the amino acid's position within one of the seven (X = 1 to 7) transmembrane segments (TMs) typically present in GPCRs. To indicate the specific position of the amino acid of interest in the respective TM, X.50 annotates the amino acid in reference to the most conserved one. Thus, one of the most crucial amino acids in ligand binding in the DR family is annotated as Asp3.32. Asp3.32, a negatively charged aspartate within the DR orthosteric binding pocket, was found to be highly conserved not only within DR members, but essentially in all aminergic GPCRs [32,41,42]. Asp3.32 represents the negatively ionizable partner of the key PI of the ligand. To successfully form this crucial ionic bond, the DR ligand needs to contain a protonable nitrogen. This is true not only for the endogenous ligand dopamine; a study by Bueschbell et al.

showed that the Asp3.32 interaction is present in essentially all D$_2$R ligands [43]. Interestingly, the ionic bond is present independently of the ligand's mode of action, i.e., agonist (such as apomorphine) or antagonist (such as haloperidol). Investigating D$_2$R, the essential ionic bond corresponds with Asp114. Another important structural element that influences ligand affinity and orientation is the serine microdomain located in TM 5 [39,42,44–46]. Ser5.42, 5.43, and 5.46 (highly conserved in the DR family) corresponding with Ser193, 194, and 197 in the D$_2$R structure form key hydrogen bonds (HBs). In dopamine binding, these HBs are formed with a catechol functional group. In other known D$_2$R ligands, HBs are present as well. However, the interaction with the serine microdomain is less dominant. This was elucidated by Bueschbell et al. showing larger distances between the serine microdomain and the ligand in the absence of catechol functionality [43]. Thus, binding affinity appears to be affected by the formation of HBs, but not necessarily by distinct amino acid interactions. Asp114 and formed HBs are responsible for ligand binding but do not determine the ligand's mode of action. However, different studies defined another microdomain, the aromatic microdomain, involved in the so-called "rotamer toggle switch", leading to receptor activation upon ligand binding [39,41,47]. This aromatic region includes amino acids like Trp6.48, Phe6.51, Phe6.52, and His/Asn6.55 corresponding to Trp386, Phe389 and 390, and His393 in D$_2$R. The involvement of the aromatic microdomain in receptor activation was also confirmed by Bueschbell et al. where known D$_2$R agonists such as dopamine, apomorphine, bromocriptine, and 7-OH-DPAT showed interactions with all crucial activating amino acids in the aromatic microdomain [43]. In contrast, antagonists like haloperidol, risperidone, or aripiprazole lacked some of the amino acid interactions. Additionally, Floresca and Schnetz also reported that amino acid residues Trp386 and His393 act as stabilizers of agonists via π–π stacking [39].
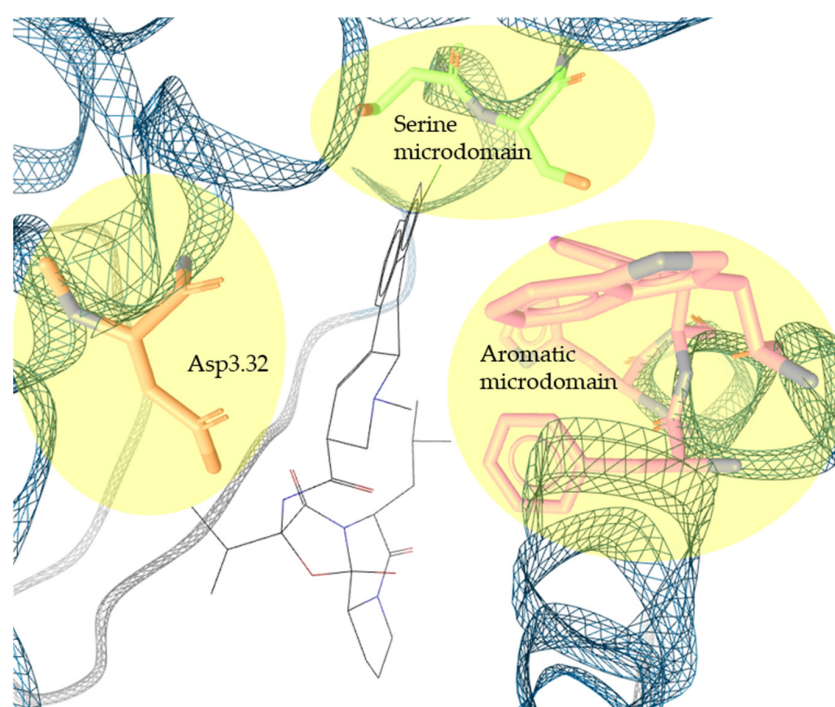
Figure 1. Overview of the highly conserved D$_2$R orthosteric binding pocket. Asp3.32, the serine microdomain, and the aromatic microdomain responsible for ligand binding, orientation, and receptor activation are highlighted. Picture generated in LigandScout (based on cryo-EM structure 7jvr [23]) showing bromocriptine in the orthosteric binding pocket.

In silico approaches need to be combined with in vitro testing for computational model validation and hit verification. Binding affinities of potential D$_2$R ligands can be investigated utilizing different in vitro methods, e.g., homogenous time-resolved fluorescence

(HTRF) assays [48,49]. This assay type is easily standardizable and commercially available for DR family members.

The aim of this study was to develop and validate high-quality in silico pharmacophore models for D_2R ligands and validate them in vitro. Providing novel D_2R ligands using our combined workflow would contribute to the discovery of novel pharmacological tools and starting points for further drug development. In Figure 2, a rational approach in identifying novel D_2R ligands is shown.
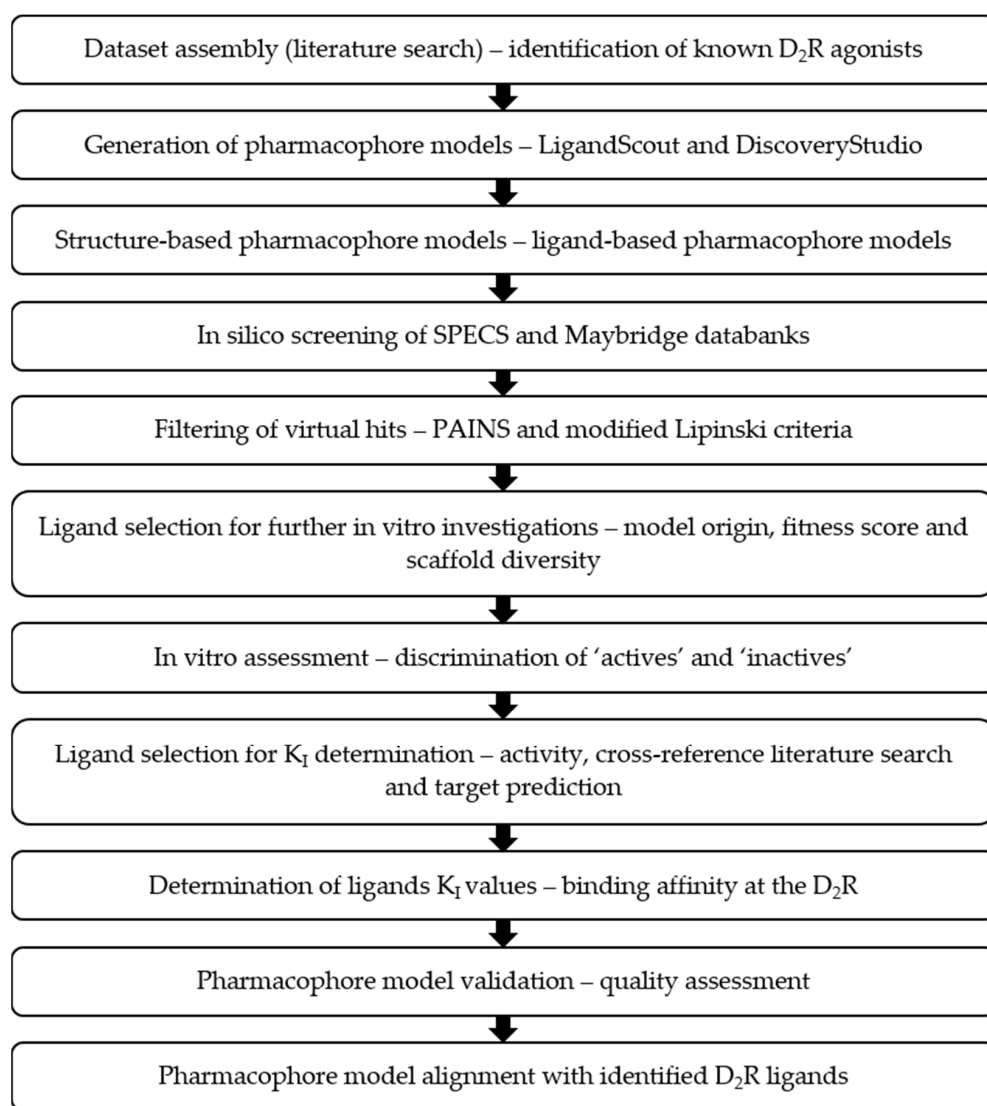
Dataset assembly (literature search) – identification of known D_2R agonists

↓

Generation of pharmacophore models – LigandScout and DiscoveryStudio

↓

Structure-based pharmacophore models – ligand-based pharmacophore models

↓

In silico screening of SPECS and Maybridge databanks

↓

Filtering of virtual hits – PAINS and modified Lipinski criteria

↓

Ligand selection for further in vitro investigations – model origin, fitness score and scaffold diversity

↓

In vitro assessment – discrimination of 'actives' and 'inactives'

↓

Ligand selection for K_I determination – activity, cross-reference literature search and target prediction

↓

Determination of ligands K_I values – binding affinity at the D_2R

↓

Pharmacophore model validation – quality assessment

↓

Pharmacophore model alignment with identified D_2R ligands

Figure 2. Combined in silico/in vitro approach to identify novel D_2R ligands.

2. Results

2.1. Dataset Assembly

To generate a high-quality dataset for the generation of the pharmacophore models, highly active D_2R ligands included in the ChEMBL database were compiled (Figure 3 and Table S1) [50–70]. The final set included 68 active compounds. The clinically used D_2R agonists (**1**–**9**) are shown in Figure 3.
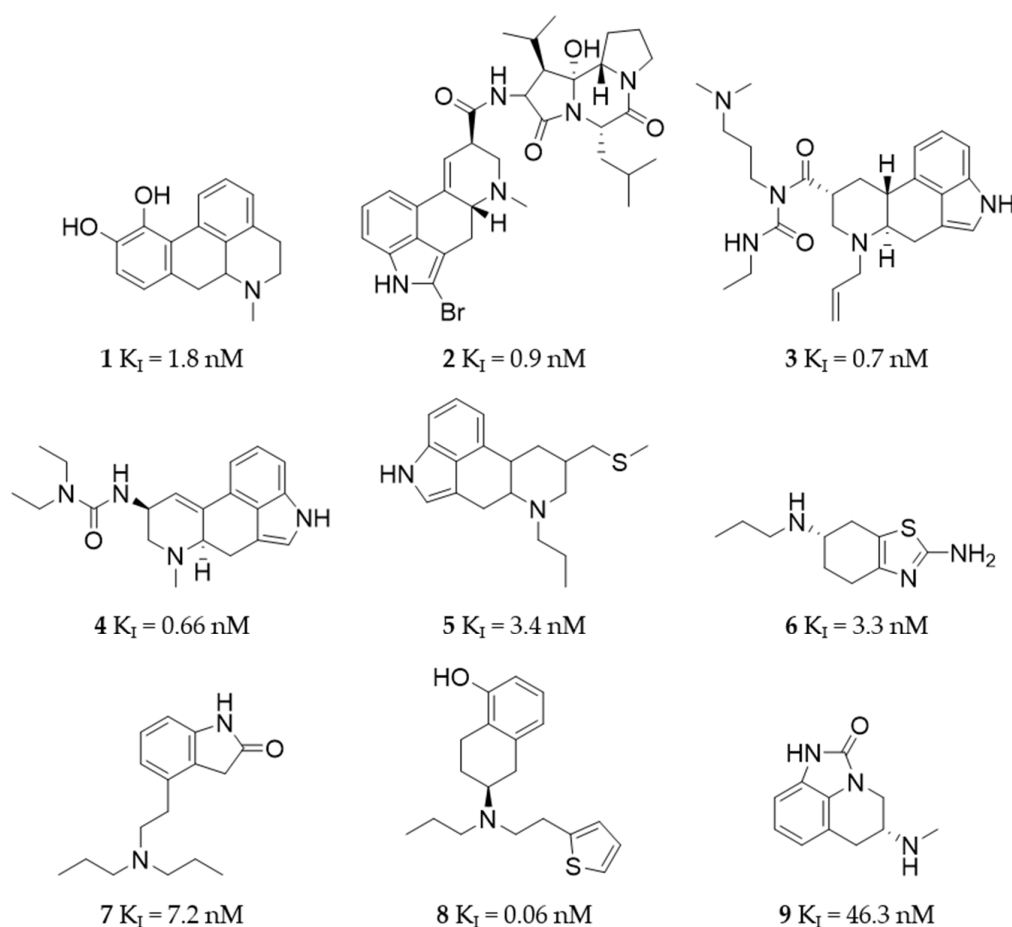
Figure 3. Overview of all clinically used D$_2$R agonists. All compounds were included in the active dataset used during the generation and validation of the developed pharmacophore models. The compounds were retrieved from the ChEMBL database including their in vitro K$_I$ values (nM).

The dataset of inactives (**SC60–SC127**) was also derived from the ChEMBL and comprised 68 compounds with a K$_I$ higher than 50 μM. The inactive dataset is shown in Table S2 [71–92]. The decoy dataset including 3752 compounds was generated utilizing the DUD-E webtool (http://dude.docking.org/ [93], accessed on 15 March 2021) and based on the structures of the active dataset.

2.2. Pharmacophore Models—LB and SB Approaches in LigandScout and DiscoveryStudio

Pharmacophore models were generated using two different software packages (LigandScout (LS) [94] and DiscoveryStudio (DS) [95]) employing SB and LB approaches. The different software packages utilize distinct screening algorithms. While the different algorithms result in different screening results, it has been shown that they are complementary, eventually increasing the coverage of the chemical space of D$_2$R ligands [96]. All pharmacophore models were initially automatically generated by the respective software. Subsequently, their individual performances were manually optimized to improve their capability of correctly distinguishing between active and inactive compounds [97]. In this step, all pharmacophore features (positively ionizable interaction (PI), hydrogen bond acceptor and donor (HBA and HBD), hydrophobic contact (HC), aromatic interaction (AI), exclusion volumes (XVOLs)) were individually optimized. Their tolerances were adapted to maximize the number of found active compounds while minimizing the number of inactive compounds and decoys, respectively. This improvement in model performance was primarily achieved by enhancing model restrictiveness, i.e., by decreasing the tolerance sphere of the PI, HBA, HBD, HC, or AI features, increasing the XVOLs' size, completely removing specific XVOLs or a selected feature. XVOLs were also added to all the models to

increase model specificity. If this additional XVOL eliminated some inactive compounds or decoys but did not result in a decrease in sensitivity, it was included. Eventually, enrichment factor (EF) and yield of actives (YoA) were used as optimization parameters during the evaluation process.

The SB models shown in Figure 4 (LS SB, M1; DS SB, M2) were both based on the recently published cryo-EM structure of D_2R in complex with agonist bromocriptine (**2**; PDB ID 7jvr [23], display of **2** in the D_2R-binding pocket (Figure 4a)). An LB model was generated in each software. The resulting models were then optimized with the datasets of actives, inactives, and decoys within their software environment. The full optimization workflow is shown in Tables S3 and S4.
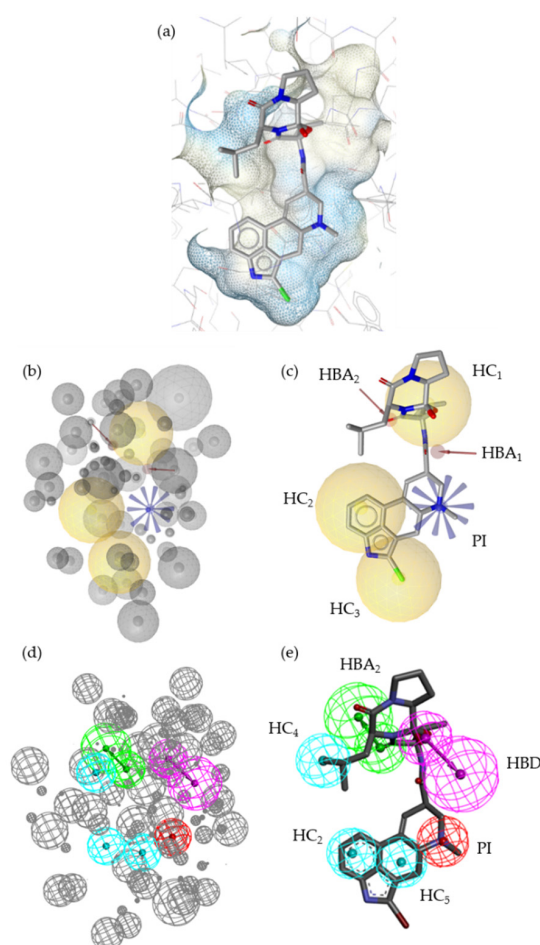

Figure 4. SB pharmacophore models M1 and M2 generated using LS and DS, respectively. M1 and M2 are based on the cryo-EM structure of D_2R in complex with agonist **2** (PDB ID 7jvr [23]). (**a**) Agonist **2** in the ligand-binding pocket of D_2R. (**b**) M1 including 60 exclusion volumes (XVOLs). (**c**) M1 aligned with **2**. (**d**) M2 including 113 XVOLs. (**e**) M2 aligned with **2**. XVOLs (grey). Hydrophobic contacts (HCs; yellow and cyan spheres). Hydrogen bond acceptor (HBA; red arrows, green spheres). Hydrogen bond donor (HBD; purple sphere). Positively ionizable interaction (PI; blue star-like shape, red sphere). All features represent characteristics of the respective structural features of the investigated molecules.

While both automatically generated models were nearly identical (Figure S1), they differed significantly after the optimization process. The SB models shared similar features (Figure 4b–e). Both SB models contained one PI feature, three HC features, and two HB features. However, the distribution of the HC features differed between the models. HC_1 was located in the tricyclic ring system in M1. In M2, HC_1 was not present. HC_2 and HC_3 were located in the tetracyclic part of **2** in M1. HC_4 was located at the isobutyl moiety of **2**

in M2. Moreover, M1 included two HBA features (HBA$_1$ and HBA$_2$) while M2 included one acceptor (HBA$_2$) and one HBD feature. The coordinates of HBA$_2$ were identical in both SB models. HBA$_1$ and HBD differed considering coordinates and feature type. Additionally, both models included distinct XVOLs, which were independently and manually optimized within LS and DS.

The LB models were based on compounds **1**, **SC52**, and **SC59** (Figure S2). Those compounds were selected since they were amongst the most active ones (K$_I$ < 2 nM), structurally diverse, and mostly not identified by M1 and M2. The LB models were generated in each software and optimized as described above (for the optimization details see Tables S5 and S6).

Although both LB models were initially based on the same compounds, they differed distinctly from the beginning (the original models are shown in Figure S3). After optimization (LS LB, M3, and DS LB, M4; Figure 5), both models contained one PI feature, two HB features, one AI feature, and at least one HC feature. While the PI features (PI$_1$ and PI$_2$) and the AI features (A$_1$ and A$_2$) were comparable to each other, other features were distinctly different between the models. Although both models featured two HBs, they were superimposed in M3, while HBA$_2$ and HBD$_2$ were clearly located at different coordinates. Furthermore, HC$_1$ and AI$_1$ in M3 were superimposed. In contrast, AI$_2$ and HC$_2$ were located at different coordinates in M4. Moreover, M4 contained an additional HC feature (HC$_3$). Comparability of the pharmacophore features models was assessed based on **SC59** which was included in the hitlist of both optimized LB models (shown in Figure S4). Additionally, both models included distinct XVOLs, which were independently and manually optimized within LS and DS.
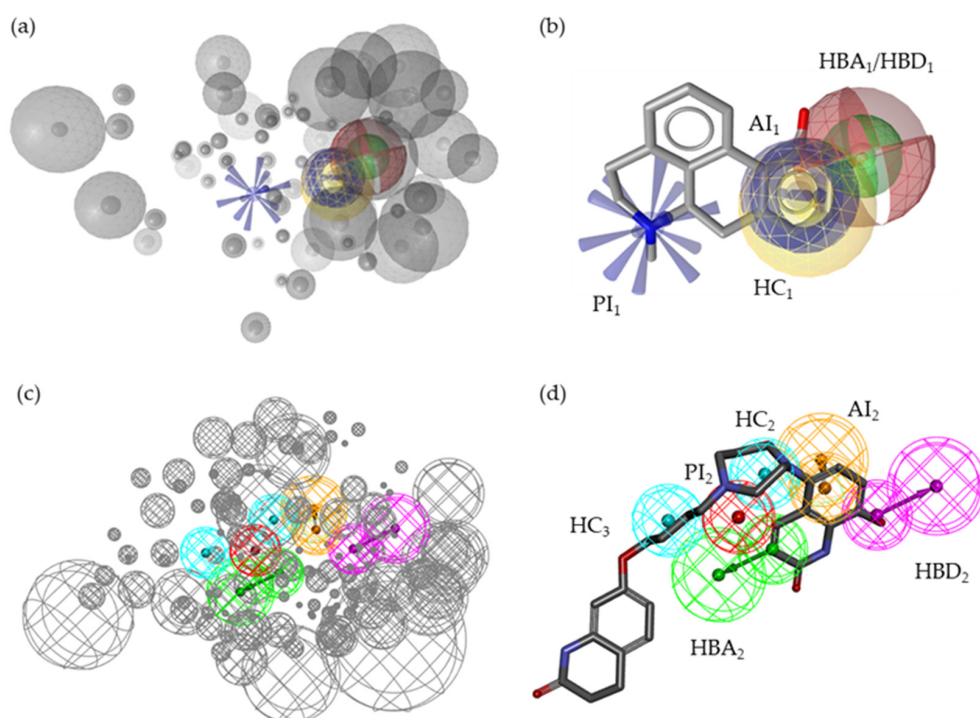

Figure 5. Ligand-based pharmacophore models M3 and M4 generated using LS and DS, respectively. Both models were based on **1**, **SC52**, and **SC59**. (**a**) Display of M3 including 61 exclusion volumes (XVOLs). (**b**) M3 aligned with **1**. (**c**) Display of M4 including 122 XVOLs. (**d**) M4 aligned with **SC59**. XVOLs (grey). Hydrophobic contacts (HCs; yellow and cyan spheres). Hydrogen bond acceptor (HBA; red and green spheres). Hydrogen bond donor (HBD; green and purple sphere). Positively ionizable interaction (PI; blue star-like shape, red sphere). Aromatic interaction (AI; blue circle, orange sphere). All features represent characteristics of the respective structural features of the investigated molecules.

In Table 1, the evaluation of the four pharmacophore models is summarized. Each model found one inactive compound. All of the models found a small number of decoys. Moreover, none of the pharmacophore models found all of the 68 active compounds. However, a sufficient yield of actives combined with small false-positive hit rates resulted in high model accuracy of all the four pharmacophore models in between 0.98 and 0.99.

Table 1. Theoretical evaluation of the generated pharmacophore models. The models were evaluated and compared to each other regarding model accuracy, enrichment factor (EF), and yield of actives (YoA). TPs, true positives. FPs, false positives. TNs, true negatives.

	M1	**M2**	**M3**	**M4**	**All Models**
Active hits (n = 68)	9	16	26	30	51
Inactive hits (n = 68)	1	0	1	0	2
Decoy hits (n = 3752)	35	36	9	27	108
TPs	9	16	26	30	51
FPs	36	36	10	27	110
TNs	3784	3783	3810	3792	3710
Specificity	0.99	0.99	1.00	0.99	0.97
Sensitivity	0.13	0.24	0.38	0.44	0.75
Accuracy	0.98	0.98	0.99	0.98	0.97
EF	11.44	17.26	41.29	29.57	18.11
YoA	0.20	0.30	0.74	0.52	0.32

While all the pharmacophore models were defined by high accuracy, they distinctly differed in EF and YoA. M3 clearly showed the highest EF as well as YoA. Moreover, all the models were characterized by high specificity and sensitivity ranging from 0.13 (M1) to 0.44 (M4). In general, the LB models M3 and M4 performed better considering all quantitative parameters. All the pharmacophore models combined identified 51 unique actives, covering 75% of the actives dataset. At the same time, only two molecules defined as inactive and 108 decoys were found by the models. While specificity, accuracy, EF, and YoA were well within the range of the separate models, the performance of the combined models was characterized by an increased sensitivity of 0.75.

2.3. Screening of the SPECS and Maybridge Databases

A total of 260,743 compounds (208,968 originating from SPECS, 51,775 originating from the Maybridge databank) were screened. All virtual hits were filtered using a "rule of five"-based physicochemical descriptor filter (Ro5; settings shown in Section 4.4) as well as the PAINS (PAINS1, 2, and 3) criteria [98,99]. Filtering resulted in 2240 hits from the different pharmacophore models. Table 2 shows the number of hits that were found by each model in the different databases. The Ro5 and PAINS filters were applied using a combined script in PipelinePilot [95].

Table 2. Summary of virtual hits after screening and filtering of the SPECS and Maybridge databases. The SPECS and Maybridge databases were screened separately with the four individual pharmacophore models generated in DS and LS. Double and triple consensus hits refer to different combinations of virtual hits from the single-hit groups.

Pharmacophore Model		Number of Hits		
		SPECS	Maybridge	Combined
Single hits	M1	236	118	354
	M2	595	76	671
	M3	157	17	174
	M4	762	78	840
Consensus hits (n = 2)	M2 + M4	122	11	133
	M1 + M3	0	0	0
	M4 + M1/M3	47	6	53
	M2 + M1/M3	10	1	11
Consensus hits (n = 3)	M2 + M4 + M1/M3	4	0	4

The compounds were ranked according to the number of models they were found by. Furthermore, virtual hits in all of the groups were sorted according to the fit score of the respective model by which they were found. In consensus hits, the model with the highest fit score was selected as a reference. Triple consensus hits, the virtual hits found by M2, M4, and M1/M3, had the highest priority. These virtual hits were followed by double consensus hits including hits from M2/M4 and M1/M3 and consensus hits from M2 and M4. No virtual hit was found by both of the LS models (M1 and M3). Consequently, category M1/M3 was introduced in the consensus hit categories, indicating the hits identified by M1 or M3. A table detailing which compounds were found by which model is shown in the Supplementary Information (Table S7). Scaffold diversity within all the groups was investigated. Similar scaffolds within one group were discarded following the principle (comparing **10–13**) shown in Figure 6.
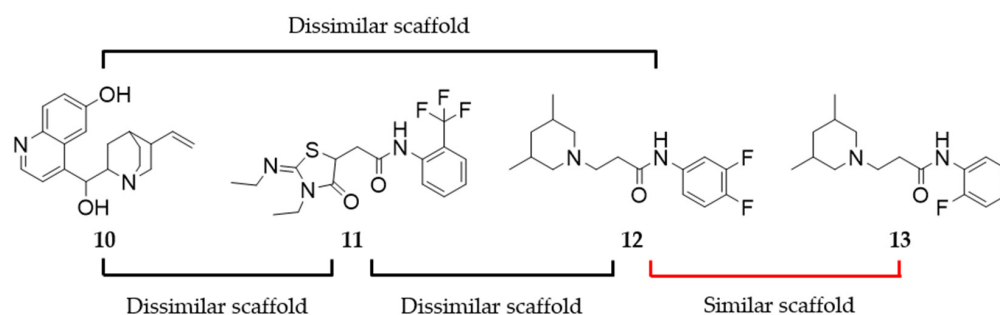

Figure 6. Exemplary assessment of scaffold similarity of consensus hits (n = 3).

Scaffold similarity was not considered between the different hit groups. Compound selection of the single-model virtual hits was conducted based on the same criteria already described considering the consensus hits. In addition to most consensus hits, 16 distinct virtual hits were selected from each model (M1–M4), allowing for balanced model validation. Scaffold similarity was additionally analyzed (Table S8 and Figure S5) applying Tanimoto scores (TS) [100], which confirmed the structural diversity of the compounds selected for biological testing. Compound **14** was prioritized for in vitro investigation because of its high similarity to the previously marketed drug octoclothepine, indicating a high probability to be a true D_2R ligand.

2.4. In Vitro Compound Screening

Activity of the selected virtual hits was investigated via competitive binding (in comparison to a fluorescence-labeled ligand) of the respective compounds at D_2R utilizing an HTRF assay. From the selected virtual hits, several compounds showed a normalized decrease in fluorescence equal or higher than 2 (Table 3). A complete summary of the in vitro binding assessment of the 90 selected virtual hits is shown in Figure S6 and Table S9, including the compound structures. All the normalized decrease in fluorescence values of the known D_2R ligands (control compounds) as well as the compounds considered active are summarized in Table 3.

Table 3. Summary of the in vitro binding assessment of the compounds considered active. All measurements were conducted at a concentration of 10 μM (n = 4). Fluorescence decrease was normalized to the control.

Compound	Normalized Decrease in Fluorescence ± SD	Compound	Normalized Decrease in Fluorescence ± SD
Control	1	**SC160**	2.41 ± 2.01
1	9.44 ± 5.97	**15**	3.99 ± 2.58
Dopamine	1.50 ± 0.88	**SC175**	2.98 ± 1.77
Sulpiride	30.65 ± 6.79	**16**	15.74 ± 18.15
2	39.10 ± 1.31	**17**	8.18 ± 3.62
Droperidol	38.69 ± 2.56	**SC191**	1.83 ± 0.83
Haloperidol	39.18 ± 0.83	**18**	10.85 ± 4.93
Piribedil	9.21 ± 3.80	**SC198**	2.43 ± 1.39
14	40.40 ± 1.39	**SC201**	1.99 ± 0.85
SC149	2.04 ± 1.34	**19**	22.08 ± 6.62
SC155	1.68 ± 0.90	**SC207**	22.89 ± 8.41

Only compound **16** showed clear discrepancies in between the replicates of the in vitro screening. Subsequently, the respective compounds were investigated considering structural novelty and lack of information about the D_2R interaction to select the most interesting candidates for K_I determination. Based on this analysis, compounds **14**, **15**, **16**, **17**, **18**, and **19** were selected for K_I determination on D_2R (the selected compounds and the potential candidates are shown in Figure 7 and Figure S10, respectively).
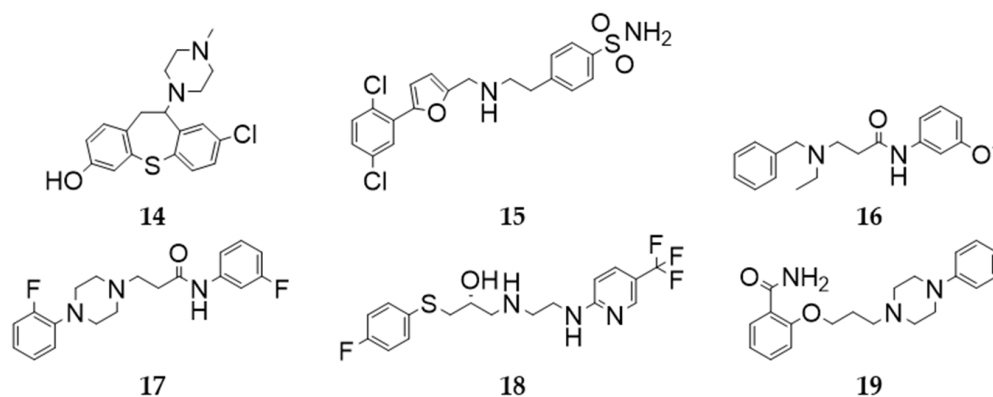

Figure 7. Two-dimensional structures of the compounds selected for in vitro K_I determination.

2.5. K_I Determination—D_2R Binding Affinity of the Selected Compounds

The selected compounds were investigated in vitro to determine their binding affinities (K_I values) at D_2R. In Figure 8, compound **14**, exerting the highest activity of all the

investigated compounds, is shown in comparison to dopamine as the endogenous D_2R ligand. The remaining compounds in comparison to dopamine are shown in Figure S7.
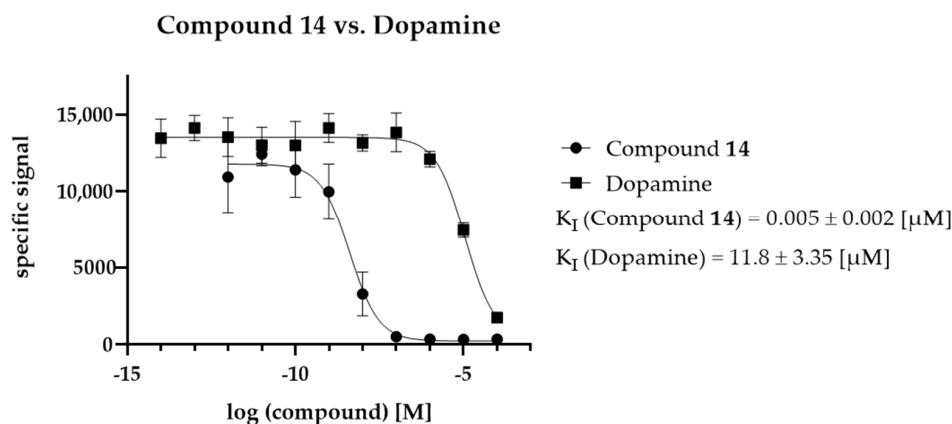
Compound 14 vs. Dopamine

Figure 8. Comparison of the K_I values of dopamine (endogenous ligand) and compound **14** (highest activity of the identified ligands). K_I values were determined with n = 6.

The activity of compound **16** was similar to that of dopamine. All the other compounds showed activities in the micromolar (compounds **15**, **17**, and **18**), submicromolar (compound **19**), and even nanomolar (compound **14**) range. The respective K_I values including their confidence intervals are shown in Table 4.

Table 4. Summary of the determined activities: K_I values of the different compounds at D_2R. Activities are also expressed as fold differences in comparison to the determined K_I of dopamine. K_I values in µM were determined using n = 6; 95% confidence intervals (CI) are shown. Dopamine is shown as the control.

Compound No. (ID)	Fold Difference	K_I (µM)	95% CI (µM)
14	2700	0.004	0.003–0.006
15	2.6	4.31	2.01–19.58
16	1.1	10.04	5.69–17.43
17	9.0	1.24	0.77–2.05
18	4.2	2.63	1.62–4.28
19	34.7	0.32	0.23–0.45
Dopamine	1	11.12	7.77–15.84

2.6. In Silico Model Evaluation

The six investigated compounds (out of 90) showed at least a similar or even higher affinity towards D_2R compared to the endogenous ligand dopamine. To analyze the quality of the in silico pharmacophore models, the hit rate (%) of each model was calculated (referring to Table S7). All the compounds but one were consensus hits from different combinations of the pharmacophore models. Only compound **18** was identified by a single model (M2). Moreover, all the four pharmacophore models identified at least one active D_2R ligand. The quantitative predictive power of the individual pharmacophore models is shown in Table 5.

Table 5. Prospective performance of the pharmacophore models generated in DS and LS.

D$_2$R Ligands (Identified by Models)	Tested Virtual Hits	Active Virtual Hits	Number of Active Hits	Hit Rate (%)
M1	22	**17**	1	4.5
M2	37	**15, 16, 17, 18**	4	10.8
M3	25	**14, 15, 19**	3	12
M4	45	**14, 16, 19**	3	6.7

While all of the generated pharmacophore models identified at least one novel D$_2$R ligand, differences could be observed between the models regarding predictive power. While M1 successfully identified one ligand, the ligand-based models M3 and M4 identified three active D$_2$R ligands. M2 identified four novel D$_2$R ligands out of the selected virtual hits. In total, the hit rate of the pharmacophore models ranged between 4.5% and 12%. According to a similarity analysis, the novel active D$_2$R ligands showed low similarity with the literature dataset (Table S11), with a maximum TC of 0.26 (compound **19** and **SC30**). Additionally, a complete Tanimoto matrix comparing all the ligands and training compounds is shown in Figure S8.

2.7. Alignment of the Pharmacophore Models with Novel D$_2$R Ligands

Structural features of the identified D$_2$R ligands were mapped to the respective pharmacophore models. Exemplarily, the mapping of compound **14** is shown in more detail in Figure 9. Both models placed the AI feature on the phenolic ring of dibenzothiepin. HC$_1$ and HC$_2$ are located at similar coordinates as the AIs in both models. HC$_3$, only present in M4, was located on the chloro-substituted ring of dibenzothiepin. The HB feature located on the hydroxy group was present in both models. However, it was defined as an HBD feature in M4, while M3 allowed both acceptor and donor features. M4 featured an additional HB feature (HBA$_2$) located on the methylated tertiary amine of piperazine. Most importantly, both models placed the PI on the connecting tertiary amine of piperazine. The mapping and alignment of compounds **15**, **16**, **17**, **18**, and **19** is available in the Supporting Information (Figures S9–S13).
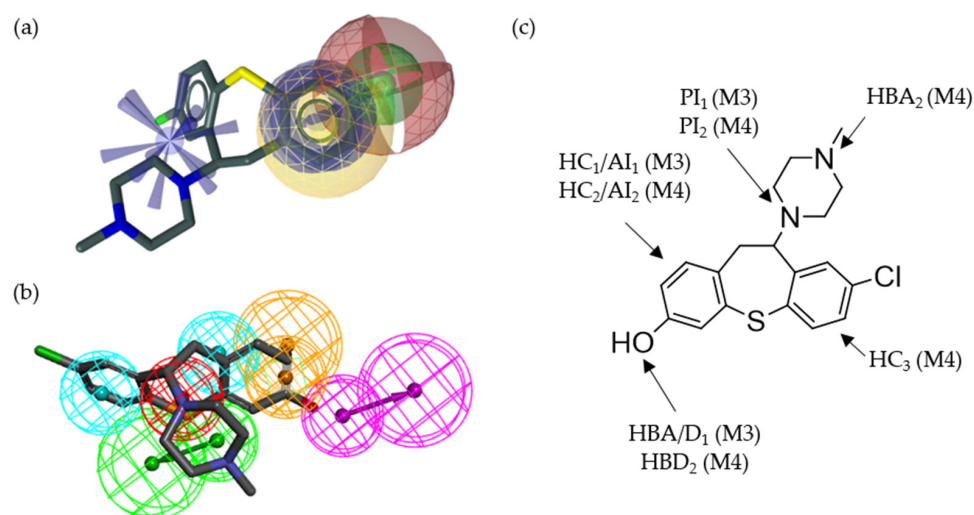

Figure 9. Display of the novel D$_2$R ligand, compound **14**, aligned with M3 and M4, identifying the compound during the screening process. (**a**) Three-dimensional structure of compound **14** including the pharmacophore features of M3. (**b**) Three-dimensional structure of compound **14** including the pharmacophore features of M4. (**c**) Two-dimensional structure of compound **14** highlighting the structural features recognized by the pharmacophore models.

2.8. Assessing the Scaffold Novelty of the Identified Ligands Compared to Known D$_2$R Ligands in ChEMBL

Comparing the identified D$_2$R ligands to their most similar ChEMBL entries, respectively, the scaffolds of compounds **14**, **17**, and **19** are already known in the literature. Compound **14** is characterized by the highest TS (0.58) since it only features an additional hydroxy group in comparison to the most similar ChEMBL entry. In compound **15**, the amine–furane–benzyl substructure is known. However, the sulfonamide functionality appears to be novel. The scaffold of compound **19** is already known in the literature. However, the ether functionality appears to be novel. Additionally, amide functional groups present in compounds **16**, **17**, and **19** are already known. An overview of the similarity analysis is shown in Figure S8 and Table S12.

3. Discussion

The theoretical evaluation of the pharmacophore models based on EF and YoA (shown in Table 1) revealed M3 as the top-ranking model. While M4 and M2 were ranked second and third (although very similar to each other regarding their performance), M1 clearly performed the worst. This evaluation of the model performances was confirmed during experimental validation (summarized in Table 5). M3 was top-ranked, with a hit rate of 12%, while M1 showed a hit rate of 4.5%. M2 and M3 were the most comprehensive models as their combined hitlist included all the active compounds (see Table S7). M4 performed equally to M3 considering the number of active compounds found during prospective screening. M1 alone identified only one active compound. There was no difference in performance regardless of whether the model was SB or LB. Most active hits (5/6) were consensus hits, suggesting that a combination of the various models increases true-positive hit rates. This synergistic effect of LB and SB screening is also in agreement with the current literature [101]. The same observation was made when investigating the synergistic combination of the different modelling environments LS and DS. Again, all the compounds except compound **18** were successfully identified due to a combination of the models generated in both programs.

Ligand novelty was investigated utilizing structure similarity searches in SciFinder searching for both identical or similar compounds and their interaction with the DR family in general and specifically D$_2$R. While the search did not yield any exact structural matches, some scaffolds have already been associated with DR activity in the literature.

A similar structure to compound **14** (SKI-417616) was investigated as a dopamine D$_4$ receptor (D$_4$R) antagonist, as well as its role in the inhibition of dengue virus replication [102]. However, the study did not investigate SKI-417616 in vitro but based its D$_4$R antagonistic potency on earlier studies investigating pyrrolobenzothiazepine derivatives [103]. However, SKI-417616 has not been investigated considering D$_2$R. Naporra et al. identified novel dibenzoxazepine and –oxepine derivatives binding to both the D$_2$R$_{long}$ and D$_2$R$_{short}$ variants. However, none of the analyzed compounds included a thioether functional group. Therefore, compound **14** represented a different scaffold. A 3D-QSAR (quantitative structure–activity relationship) study presented a retrospective study based on known D$_2$R and D$_4$R antagonists. However, the investigated compounds, again, did not include the thioether group present in compound **14**. The role of similar compounds acting as insecticides through D$_1$R antagonism was investigated by Meyer et al. This study focused only on non-human DRs from the mosquito *Aedes aegypti* [104–106]. In agreement with the SciFinder literature search, the most similar compound found (shown in Table S12) was octoclothepine (**SC209**, brand names Clotepin and Clopiben), a highly potent D$_2$R antagonist that was also clinically used for a short time in 1971 for the treatment of schizophrenic psychosis [107].

Compound **15** has not been reported as a DR ligand according to the SciFinder results. **SC210**, the most similar compound found in ChEMBL (4-(5-(((2-(5-fluoro-1*H*-pyrrolo[2,3-b]pyridin-3-yl)ethyl)amino)methyl)furan-2-yl)phenol, TS of only 0.21) was an antagonist for D$_2$R identified in a virtual screening campaign investigating serotonin receptors [108].

Referring to the similarity search in ChEMBL utilizing the Tanimoto matrix shown in Table S12, both compounds **16** and **17** showed the highest structural similarity with the same compound, **SC211**, a piperazine benzamide derivative (3-(4-(4-chlorophenyl)piperazin-1-yl)-N-(3-methoxyphenyl)propanamide, CHEMBL329228). Interestingly, the identified compound has been shown to possess high affinity and selectivity towards D_4R [109]. Considering compound **18**, similarity searches in ChEMBL resulted in finding the most similar structure to be 1-(3-((4-fluorophenyl)thio)propyl)-4-(4-(trifluoromethyl)phenyl)piperazine (**SC212**, ChEMBL1940410), a haloperidol derivative. This compound has been associated with atypical antipsychotic activity [110]. Interestingly, compound **18** yielded the lowest TS of all the novel D_2R ligands, with only 0.19. While it is clearly active at D_2R, it also represents the most novel scaffold, closely followed by compound **15**.

Considering compound **19**, the ligand also has not been discussed in the literature yet. However, similar structures have been investigated, analyzing their role as D_3R-selective compounds and D_2R antagonists according to a SciFinder search [111]. Additionally, ChEMBL cross-referencing resulted in a highly similar compound **SC213** (1-(3-phenoxypropyl)-4-phenylpiperazine, ChEMBL1940414) missing the amide functional group, while the remaining structure was identical. **SC213** originates from the same source as **SC211** where both entries are shown to be based on haloperidol, a potent D_2R antagonist [110]. Considering the novel D_2R ligands which were identified, scaffold similarity searches and literature cross-referencing indicated a potential role not just as D_2R ligands, but also as other DR family members. Moreover, the referenced studies highlight the antagonistic mode of action for most of the compounds discussed above.

The PI is a key feature in all the active compounds represented by the basic nitrogen atom. This is highlighted in the alignments shown in Figures 9 and S9–S13. Two of the novel compounds, **14** and **18** (shown in Figures 9 and S12), include a hydroxy functional group, potentially interacting with the serine microdomain. All of the other novel compounds contain at least two or even three structural elements enabling other HB interactions, e.g., amide or sulfonamide functional groups. The presence of such alterative binding modes rationalizes the necessity of complementary pharmacophore models for comprehensive virtual screening campaigns.

The developed combined workflow focused on the identification of ligands binding to D_2R. This can be seen as the first step in a drug discovery campaign. From a therapeutic point of view, D_2R agonists and antagonists are interesting agents for the treatment of different diseases as described above. Therefore, the developed workflow combined with HTRF assays can be a valuable starting point in future studies. Follow-up projects specifically investigating a(nta)gonistic behavior as well as receptor promiscuity issues addressed earlier will be conducted based on the identified D_2R ligands. Those projects will also involve combinational approaches of in silico and in vitro tools. The already established HTRF principle presented in this manuscript will also enable in vitro selectivity quantification for D_2R-related GPCRs; e.g., against D_1R, D_3R, serotonin, and adenosine receptors. Quantifying a ligand's mode of action in vitro will require functional assays, potentially involving downstream signal quantification; e.g., Ca^{2+} flux or cAMP levels in cell-based setups.

Summarizing, we could confirm our original hypothesis showing that a high-quality combined in silico/in vitro approach enables efficient identification of novel D_2R ligands. Questions like selectivity and mode of action of ligands still need to be addressed. Furthermore, they could drive the development of pharmacological tools, improving drug design processes in D_2R-associated pathological conditions.

4. Materials and Methods

The general workflow used to follow a rational experimental design is shown in Figure 2.

4.1. Materials

Dopamine hydrochloride, (*S*)-(−)-sulpiride, dimethyl sulfoxide (DMSO), and droperidol were all acquired from Sigma-Aldrich. Haloperidol and piribedil were both acquired from TCI Chemicals. Bromocriptine mesylate was acquired from VWR. Apomorphine hydrochloride was kindly provided by EVERPharma AT GmbH within the context of a different project. Tested compounds (shown in Table S9) were acquired either from SPECS (https://www.specs.net/, accessed in April 2021) or Maybridge (https://www.thermofisher.com/at/en/home/industrial/pharma-biopharma/drug-discovery-development/screening-compounds-libraries-hit-identification.html, accessed in April 2021). All the compounds were dissolved in DMSO, aliquoted, and stored at −80 °C until further use.

4.2. Dataset Assembly

The dataset assembly was based on a literature search of D_2R ligands in the ChEMBL databank. Using ChEMBL, a set of actives (entries shown in Figure 3 and Table S1), inactives, and decoys was generated. The dataset was specifically filtered for D_2R agonists with binding affinities of up to 500 nM. During dataset assembly, each ChEMBL entry and its corresponding publication was investigated considering binding affinity, methodological approach, and determination of D_2R agonism. Finally, 68 ChEMBL entries including nine approved D_2R agonists with binding affinity ranging from 0.075 nM up to 338 nM were used. The set of active compounds only compiled compounds with biological activities investigated in vitro. The set of inactives included 68 entries with binding affinities above 50 μM. The decoy dataset was generated utilizing the DUD-E webtool (http://dude.docking.org/, accessed on 15 March 2021) to create 3752 decoys based on the actives set. DS was used to ensure correctness of conformations, add hydrogens to the structures, and minimize the datasets. Datasets were generated using the "BEST settings", with a maximum of 255 conformations per molecule in DS.

In LS screening, datasets were generated using the "iCon [112]-best" settings with a maximum of 200 conformations per molecule.

4.3. Generation of Pharmacophore Models

4.3.1. SB Pharmacophore

SB pharmacophore models were based on the cryo-EM structure of D_2R bound to agonist **2** (PDB ID 7jvr). In LS, a pharmacophore was created and transferred into the screening perspective. The original pharmacophore model was edited in a step-wise manner by altering feature tolerance and creation of new XVOLs. The different models were used to screen actives, inactives and decoy datasets maximizing recognition of actives while minimizing recognition of inactives and decoys. The pharmacophore model generated in DS was optimized using the same workflow.

4.3.2. LB Pharmacophore

LB pharmacophore models generated in LS were based on the active compounds previously not identified by the LS SB model. Compounds **1**, **SC52**, and **SC59** were used to generate a shared feature pharmacophore model. Conformers were generated using the standard BEST setting. The resulting pharmacophore models were then optimized in the same way as the SB LS model. The generation of the LB model in DS was based on the same compounds as the LS model to increase comparability. The pharmacophore model generated in DS was optimized using the same workflow.

4.3.3. Pharmacophore Model Validation Metrics

The quality of pharmacophore models is described by several parameters [113]. The most frequent are sensitivity (Equation (1)) and specificity (Equation (2)). Sensitivity expresses the probability of a randomly selected active compound to map the model. Specificity, on the other hand, describes the probability that a randomly selected inactive compound will not map the model.

$$\text{Sensitivity} = \text{number of actives identified by the model/number of actives in the dataset} \tag{1}$$

$$\text{Specificity} = \text{number of actives not identified by the model/number of inactives in the dataset} \tag{2}$$

Additionally, pharmacophore models are frequently described by parameters such as yield of actives (YoA), enrichment factor (EF), and accuracy. YoA (Equation (3)) specifies the ratio of true positives identified by the model to the number of all the compounds that mapped the model. EF (Equation (4)) as opposed to yield of actives also takes into account database sizes of active and inactive compounds, as well as of decoys. Accuracy refers to the probability of any compound being correctly classified either as active or inactive by the model (Equation (5)).

$$\text{YoA} = \text{number of true positives/number of total hits} \tag{3}$$

$$\text{EF} = \text{YoA/(number of actives in the database/number of all the compounds in the database)} \tag{4}$$

$$\text{Accuracy} = \text{(number of true positives + number of true negatives)/number of all the compounds in the database} \tag{5}$$

Eventually, EF and YoA were utilized for evaluating the optimization process.

4.4. Predictive Screening—SPECS and Maybridge

SPECS (Specs_SC_10mg_Apr2021; 208,968 compounds) and Maybridge (MayBridge HitDiscover database; downloaded in April 2021, 51,775 compounds) databases were screened in the respective software used for the generation of the pharmacophore models. After the screening, the resulting virtual hits were processed in PipelinePilot applying a PAINS and Ro5-based physicochemical descriptor filter (Table 6). The limits for the physicochemical parameters were based on a detailed structural analysis of all the active compounds (compounds **1**–**9** and **SC1**–**SC59**) utilized during the pharmacophore model generation. Regarding PAINS, three different filters, PAINS1, 2, and 3, were applied using default settings [98,99]. PAINS filtering was followed by physicochemical descriptor filtering applying the criteria shown in Table 6.

Table 6. Summary of the parameter restrictions applied during physicochemical descriptor filtering prior to virtual hit selection.

Parameter	Value
Molecular weight (MW) (g/mol)	$600 \geq x \geq 200$
cLogP	$6.0 \geq x \geq 1.5$
HB acceptors	$7 \geq x \geq 0$
HB donors	$3 \geq x \geq 0$
Rotatable bonds	$18 \geq x \geq 0$
Rings	$5 \geq x \geq 2$
Aromatic rings	$3 \geq x \geq 1$

Virtual hits meeting the PAINS and physicochemical descriptor criteria were further considered regarding ligand selection and in vitro investigation.

4.5. Settings for an HTRF-Compatible Tecan Spark Plate Reader

All the HTRF assays were performed using a Tecan Spark plate reader. The respective settings were specifically modified and optimized for the determination of D_2R ligand-binding affinities. Experiments were performed using two different emission wavelengths at 620 and 665 nm, respectively, subsequently used for quantifying binding affinities. Fluorophores were excited at 320 nm. A Dichroic 510 mirror was used, while lag and integration times of 100 and 400 μs were applied, respectively. Flashes were set to 75.

Electronic gain was automatically optimized, while the z-position was optimized based on the well with the highest expected signal. Experiments described in 4.6, 4.8, and 4.10 require the use of two 96-well plates. The first plate was used to determine the gain and the z-position. Subsequently, the determined values were set manually for the second plate to enable direct comparison between the different plates.

4.6. Characterization of D₂R Carrier Cells—KD Determination

The cells used for the subsequent screening and detailed investigation of D$_2$R ligands were acquired from PerkinElmer/cisbio (Tag-lite Dopamine D2-labeled Cells, ready-to-use (transformed and labeled), 200 tests; C1TT1D2). The cells were stored in liquid nitrogen until further use. Fluorescent ligand (Dopamine D2 Receptor red antagonist Fluorescent Ligand, stored at −20 °C; L0002RED), assay buffer (Tag-lite Buffer (5× concentrate), 100 mL, stored at 4 °C; LABMED), and 96-well plates (HTRF 96-well low-volume white plate; 66PL96005) required for the in vitro assay were also acquired from PerkinElmer/cisbio. Bromocriptine mesylate (50 mg; CAYM14598-50) was acquired from VWR. The assay was conducted according to the standard operation protocol (SOP) available from PerkinElmer/cisbio. The 96-well plates were incubated at room temperature for 2 h. The 96-well plates were read on a Tecan Spark plate reader (the settings are shown in Section 4.5). The respective concentrations of the dilution series were performed in triplicates. In total, K$_D$ determination was performed three times.

4.7. Compound Selection for Assessing In Vitro Activity

Ligand selection regarding activity screening was performed using fitness score, scaffold similarity, and model origin as a selection matrix. Thus, ligands found by the different pharmacophore models (consensus hits) were prioritized. Consensus hits were categorized as the hits found by M2 + M4 + M1/M3 (triple consensus), M2 + M4, M2 + M1/M3, or M4 + M1/M3 (double consensus). Single hits originating from only one of the pharmacophore models were selected in a balanced manner to enable validation of the respective models later on. Structural diversity was assessed using DataWarrior [114] based on linker regions, ring sizes, number of rings, and functional groups. Considering similar compounds, compounds with lower fitness scores were excluded from the selection.

4.8. In Vitro Assessment of Compound Activity

Materials described in 4.6 were also used during ligand screening. TLB (1×) was prepared as described earlier. For ligand screening, compounds were prepared at a working solution concentration of 40 μM in 1× TLB. Known D$_2$R ligands (both agonists and antagonists) were used as the positive controls at the same concentration. The assay was conducted according to the SOP available from PerkinElmer/cisbio. The 96-well plates were incubated at room temperature in the dark for 2 h. The 96-well plates were read on a Tecan Spark plate reader (the settings are shown in Section 4.5). In total, ligand screening was performed twice.

4.9. Ligand Selection for Detailed In Vitro Investigation (K$_I$ Determination)

Ligands were considered active when they had a DNF of $\geq$ 2 compared to the control. Active ligands were investigated using a literature cross-reference search (SciFinder) and predicting the compounds' most likely molecular targets (SwissTargetPrediction). In SciFinder, a database of all publications based on the search phrase "dopamine receptor" was generated. Active ligands were cross-referenced using their exact structure as well as similar structures (similarity score of $\geq$80) with the literature database. Exact structural matches with a known activity at D$_2$R were automatically excluded from the selection. Similarity matches were considered as candidates. Swiss target prediction was used to refine compound selection based on the SciFinder search. Therefore, compounds of interest were investigated considering their probability to interact with the DR family as well as the availability of structurally similar compounds (focusing on 2D structures). The results

from the Swiss target prediction analysis were evaluated based on the decision tree shown in Figure 10.
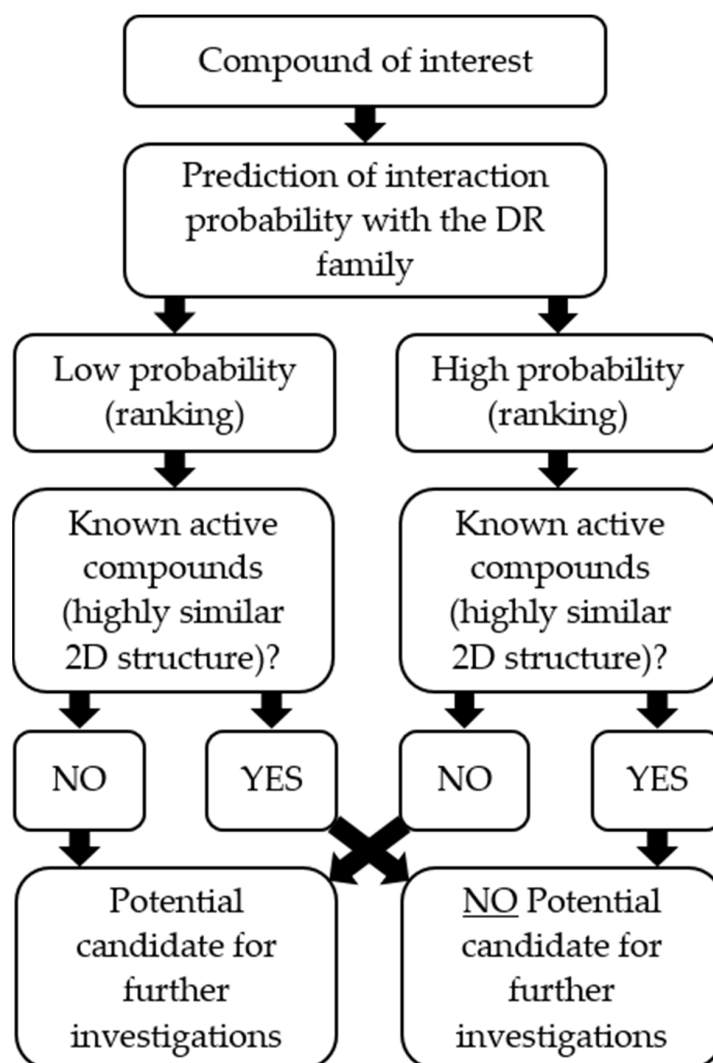

Figure 10. Decision tree following the investigation of the compounds of interest based on a SwissTargetPrediction search.

Finally, the candidates were sorted by activity and investigated considering scaffold diversity.

4.10. K_I Determination of the Selected Ligands

The materials described in 4.6 were also used during K_I determination of the ligands selected after screening. The selected ligands (compounds **14**, **15**, **16**, **17**, **18**, and **19**) were diluted in $1\times$ TLB. Compounds **14**, **15**, **18**, and **19** were diluted to an initial working solution concentration of 4×10^{-4} M. Compound **15** was diluted to an initial working solution concentration of 4×10^{-5} M. Compound **16** was diluted to an initial working solution concentration of 1×10^{-4} M. Different concentrations were chosen due to differences in aqueous solubility of the compounds. K_I was determined following the SOP available at PerkinElmer/cisbio. The 96-well plates were incubated at room temperature in the dark for 2 h. The 96-well plates were read on a Tecan Spark plate reader (the settings are shown in Section 4.5). In total, K_I determination was performed twice.

4.11. Pharmacophore Model Evaluation

The theoretical model validation was based on the metrics described in Section 4.3.3. The prospective performance was evaluated based on the models' predictive power identifying previously unknown D_2R ligands. It was quantified as the hit rate (%).

4.12. Assessing Scaffold Similarity/Dissimilarity

Canonical SMILES codes of all the compounds of interest were imported to Canvas 3.8. In Canvas 3.8, radial fingerprints (ECFP4 [115,116]) of all the molecules (based on 2D structures) were calculated followed by an automated calculation of a TS [100] for each compared pair. TS matrices were exported to Excel as .csv files and imported to GraphPad Prism 8 to display heatmaps, color-coding the structural similarities. TSs range from 0 to 1. An increasing coefficient indicated an increasing structural similarity. In each similarity assessment, the 2D structures of the most similar compound pairs were observed in detail to investigate compound novelty and scaffold diversity.

4.13. Data Processing, Representation, and Analysis

Pharmacophore modelling and virtual screening were performed in LS version 4.4.5 (Inte:Ligand GmbH, Vienna, Austria) and DS 2018 (DS, Accelrys Inc., San Diego, CA, USA). Two-dimensional structures of all the compounds were generated in ChemDraw 19.0 (PerkinElmer, Waltham, MA, USA). Sd files used for similarity assessments were generated in PipelinePilot Client 9.1 [95] and processed in Canvas 3.8 (Canvas, Schrödinger, LLC, New York, NY, USA, 2021) and DataWarrior [114]. Heatmaps, NDF, and saturation curves were processed and visualized in GraphPad Prism 8.

Supplementary Materials: The following are available online at https://www.mdpi.com/article/10.3390/molecules27144435/s1, Table S1: Dataset of active compounds, Table S2: Dataset of inactives, Table S3: Evaluation of the optimization process of model M1, Table S4: Evaluation of the optimization process of model M2, Table S5: Evaluation of the optimization process of model M3, Table S6: Evaluation of the optimization process of model M4, Table S7: Selection of virtual hits after virtual screening, Table S8: Similarity assessment comparing the selected virtual hits, Table S9: Summary of the compounds selected for further in vitro investigation, Table S10: Overview of in vitro activity screening of all the selected virtual hits, Table S11: Similarity assessment comparing the identified ligands and the dataset of actives, Table S12: Assessment of ligand novelty compared to ChEMBL entries, Figure S1: Original SB pharmacophore models, Figure S2: Active compounds used for LB pharmacophore approaches, Figure S3: Original LB pharmacophore models, Figure S4: Alignment of LB models with **SC59**, Figure S5: Overview of similarity assessments in single- and consensus-hit groups, Figure S6: Overview of in vitro activity screening of all the selected virtual hits, Figure S7: Overview of K_I values of the identified ligands, Figure S8: Assessment of scaffold diversity comparing the identified ligands and the dataset of actives, Figure S9: Alignment of compound **15** with M2 and M3, Figure S10: Alignment of compound **16** with M2 and M4, Figure S11: Alignment of compound **17** with M1 and M2, Figure S12: Alignment of compound **18** with M2, Figure S13: Alignment of compound **19** with M3 and M4.

Author Contributions: Conceptualization, D.S.; methodology, C.L., J.K. and L.Z.; software, commercially and publicly available software was used; validation, D.S., J.K., L.Z. and V.T.; investigation, C.L., J.K. and L.Z.; data curation, J.K. and L.Z.; writing—original draft preparation. C.L., J.K. and L.Z.; writing—review and editing. D.S., J.K., L.Z. and V.T.; visualization. J.K. and L.Z.; supervision, D.S. and V.T.; project administration. D.S. All authors have read and agreed to the published version of the manuscript.

Institutional Review Board Statement: Not applicable.

Informed Consent Statement: Not applicable.

Data Availability Statement: The data presented in this study are available in Supplementary Material. If further data are required, they are available from the corresponding author upon request.

Conflicts of Interest: The authors declare no conflict of interest.

Sample Availability: Samples of the compounds are not available from the authors.

References

1. Hauser, A.S.; Attwood, M.M.; Rask-Andersen, M.; Schioth, H.B.; Gloriam, D.E. Trends in GPCR drug discovery: New agents, targets and indications. *Nat. Rev. Drug Discov.* **2017**, *16*, 829–842. [CrossRef] [PubMed]
2. Azam, S.; Haque, M.E.; Jakaria, M.; Jo, S.H.; Kim, I.S.; Choi, D.K. G-Protein-Coupled Receptors in CNS: A Potential Therapeutic Target for Intervention in Neurodegenerative Disorders and Associated Cognitive Deficits. *Cells* **2020**, *9*, 506. [CrossRef] [PubMed]
3. Hauser, A.S.; Chavali, S.; Masuho, I.; Jahn, L.J.; Martemyanov, K.A.; Gloriam, D.E.; Babu, M.M. Pharmacogenomics of GPCR Drug Targets. *Cell* **2018**, *172*, 41–54.e19. [CrossRef] [PubMed]
4. Pan, X.; Kaminga, A.C.; Wen, S.W.; Wu, X.; Acheampong, K.; Liu, A. Dopamine and Dopamine Receptors in Alzheimer's Disease: A Systematic Review and Network Meta-Analysis. *Front. Aging Neurosci.* **2019**, *11*, 175. [CrossRef]
5. Stocchi, F.; Torti, M.; Fossati, C. Advances in dopamine receptor agonists for the treatment of Parkinson's disease. *Expert Opin. Pharmacother.* **2016**, *17*, 1889–1902. [CrossRef]
6. Li, P.; Snyder, G.L.; Vanover, K.E. Dopamine Targeting Drugs for the Treatment of Schizophrenia: Past, Present and Future. *Curr. Top. Med. Chem.* **2016**, *16*, 3385–3403. [CrossRef]
7. Martel, J.C.; Gatti McArthur, S. Dopamine Receptor Subtypes, Physiology and Pharmacology: New Ligands and Concepts in Schizophrenia. *Front. Pharmacol.* **2020**, *11*, 1003. [CrossRef]
8. Carbone, F.; Djamshidian, A.; Seppi, K.; Poewe, W. Apomorphine for Parkinson's Disease: Efficacy and Safety of Current and New Formulations. *CNS Drugs* **2019**, *33*, 905–918. [CrossRef]
9. Smith, Y.; Wichmann, T.; Factor, S.A.; DeLong, M.R. Parkinson's disease therapeutics: New developments and challenges since the introduction of levodopa. *Neuropsychopharmacology* **2012**, *37*, 213–246. [CrossRef]
10. Kuo, J.; Hwu, H.G. Aripiprazole and haloperidol: Beneficial combination antipsychotic therapy for a schizophrenic patient. *Clin. Neuropharmacol.* **2008**, *31*, 173–175. [CrossRef]
11. Thanvi, B.R.; Lo, T.C. Long term motor complications of levodopa: Clinical features, mechanisms, and management strategies. *Postgrad Med. J.* **2004**, *80*, 452–458. [CrossRef] [PubMed]
12. Tambasco, N.; Romoli, M.; Calabresi, P. Levodopa in Parkinson's Disease: Current Status and Future Developments. *Curr. Neuropharmacol.* **2018**, *16*, 1239–1252. [CrossRef] [PubMed]
13. Sykes, D.A.; Moore, H.; Stott, L.; Holliday, N.; Javitch, J.A.; Lane, J.R.; Charlton, S.J. Extrapyramidal side effects of antipsychotics are linked to their association kinetics at dopamine D2 receptors. *Nat. Commun.* **2017**, *8*, 763. [CrossRef] [PubMed]
14. Berman, B.D. Neuroleptic malignant syndrome: A review for neurohospitalists. *Neurohospitalist* **2011**, *1*, 41–47. [CrossRef] [PubMed]
15. Wang, Q.; Mach, R.H.; Luedtke, R.R.; Reichert, D.E. Subtype selectivity of dopamine receptor ligands: Insights from structure and ligand-based methods. *J. Chem. Inf. Model.* **2010**, *50*, 1970–1985. [CrossRef]
16. Butini, S.; Nikolic, K.; Kassel, S.; Bruckmann, H.; Filipic, S.; Agbaba, D.; Gemma, S.; Brogi, S.; Brindisi, M.; Campiani, G.; et al. Polypharmacology of dopamine receptor ligands. *Prog. Neurobiol.* **2016**, *142*, 68–103. [CrossRef]
17. Prasad, M.E.; Hung, S.Y. Current Therapies in Clinical Trials of Parkinson's Disease: A 2021 Update. *Pharmaceuticals* **2021**, *14*, 717. [CrossRef]
18. Basith, S.; Cui, M.; Macalino, S.J.Y.; Park, J.; Clavio, N.A.B.; Kang, S.; Choi, S. Exploring G Protein-Coupled Receptors (GPCRs) Ligand Space via Cheminformatics Approaches: Impact on Rational Drug Design. *Front. Pharmacol.* **2018**, *9*, 128. [CrossRef]
19. Wang, S.; Che, T.; Levit, A.; Shoichet, B.K.; Wacker, D.; Roth, B.L. Structure of the D2 dopamine receptor bound to the atypical antipsychotic drug risperidone. *Nature* **2018**, *555*, 269–273. [CrossRef]
20. Im, D.; Inoue, A.; Fujiwara, T.; Nakane, T.; Yamanaka, Y.; Uemura, T.; Mori, C.; Shiimura, Y.; Kimura, K.T.; Asada, H.; et al. Structure of the dopamine D2 receptor in complex with the antipsychotic drug spiperone. *Nat. Commun.* **2020**, *11*, 6442. [CrossRef]
21. Fan, L.; Tan, L.; Chen, Z.; Qi, J.; Nie, F.; Luo, Z.; Cheng, J.; Wang, S. Haloperidol bound D2 dopamine receptor structure inspired the discovery of subtype selective ligands. *Nat. Commun.* **2020**, *11*, 1074. [CrossRef] [PubMed]
22. Yin, J.; Chen, K.M.; Clark, M.J.; Hijazi, M.; Kumari, P.; Bai, X.C.; Sunahara, R.K.; Barth, P.; Rosenbaum, D.M. Structure of a D2 dopamine receptor-G-protein complex in a lipid membrane. *Nature* **2020**, *584*, 125–129. [CrossRef] [PubMed]
23. Zhuang, Y.; Xu, P.; Mao, C.; Wang, L.; Krumm, B.; Zhou, X.E.; Huang, S.; Liu, H.; Cheng, X.; Huang, X.P. Structural insights into the human D1 and D2 dopamine receptor signaling complexes. *Cell* **2021**, *184*, 931–942.e18. [CrossRef]
24. Lemos, A.; Melo, R.; Preto, A.J.; Almeida, J.G.; Moreira, I.S.; Dias Soeiro Cordeiro, M.N. In Silico Studies Targeting G-protein Coupled Receptors for Drug Research Against Parkinson's Disease. *Curr. Neuropharmacol.* **2018**, *16*, 786–848. [CrossRef] [PubMed]
25. Sharma, V.W.S.; Kumar, H. Structure- and ligand-based drug design: Concepts, approaches, and challenges. In *Chemoinformatics and Bioinformatics in the Pharmaceutical Sciences*; Sharma, H.N.O., Raghav, P.W., Goyal, R.K., Eds.; Elsevier: Amsterdam, The Netherlands, 2021; pp. 27–53.
26. Lian, P.; Xu, L.; Geng, C.; Qian, Y.; Li, W.; Zhen, X.; Fu, W. A computational perspective on drug discovery and signal transduction mechanism of dopamine and serotonin receptors in the treatment of schizophrenia. *Curr. Pharm. Biotechnol.* **2014**, *15*, 916–926. [CrossRef]

27. Ishiki, H.M.; Filho, J.M.B.; da Silva, M.S.; Scotti, M.T.; Scotti, L. Computer-aided Drug Design Applied to Parkinson Targets. *Curr. Neuropharmacol.* **2018**, *16*, 865–880. [CrossRef] [PubMed]

28. Ostopovici-Halip, L.; Rad-Curpan, R. Modeling of ligand binding to the dopamine D2 receptor. *J. Serbian Chem. Soc.* **2014**, *79*, 175–183. [CrossRef]

29. Malo, M.; Brive, L.; Luthman, K.; Svensson, P. Investigation of D(2) receptor-agonist interactions using a combination of pharmacophore and receptor homology modeling. *ChemMedChem* **2012**, *7*, 471–482. [CrossRef]

30. Penjisevic, J.Z.; Sukalovic, V.V.; Andric, D.B.; Roglic, G.M.; Novakovic, I.T.; Soskic, V.; Kostic-Rajacic, S.V. Synthesis, biological evaluation and docking analysis of substituted piperidines and (2-methoxyphenyl)piperazines. *J. Serbian Chem. Soc.* **2016**, *81*, 347–356. [CrossRef]

31. Penjisevic, J.Z.; Sukalovic, V.V.; Andric, D.B.; Roglic, G.M.; Soskic, V.; Kostic-Rajacic, S.V. Synthesis, Biological, and Computational Evaluation of Substituted 1-(2-Methoxyphenyl)-4-(1-phenethylpiperidin-4-yl)piperazines and 1-(2-Methoxyphenyl)-4-[(1-phenethylpiperidin-4-yl)methyl]piperazines as Dopaminergic Ligands. *Arch. der Pharm.* **2016**, *349*, 614–626. [CrossRef]

32. Platania, C.B.; Salomone, S.; Leggio, G.M.; Drago, F.; Bucolo, C. Homology modeling of dopamine D2 and D3 receptors: Molecular dynamics refinement and docking evaluation. *PLoS ONE* **2012**, *7*, e44316. [CrossRef] [PubMed]

33. Ortore, G.; Tuccinardi, T.; Bertini, S.; Martinelli, A. A theoretical study to investigate D2DAR/D4DAR selectivity: Receptor modeling and molecular docking of dopaminergic ligands. *J. Med. Chem.* **2006**, *49*, 1397–1407. [CrossRef] [PubMed]

34. Sukalovic, V.; Andric, D.; Roglic, G.; Kostic-Rajacic, S.; Schrattenholz, A.; Soskic, V. Synthesis, dopamine D2 receptor binding studies and docking analysis of 5-[3-(4-arylpiperazin-1-yl)propyl]-1H-benzimidazole, 5-[2-(4-arylpiperazin-1-yl)ethoxy]-1H-benzimidazole and their analogs. *Eur. J. Med. Chem.* **2005**, *40*, 481–493. [CrossRef] [PubMed]

35. Sukalovic, V.; Soskic, V.; Andric, D.; Roglic, G.; Kostic-Rajacic, S. Modeling key interactions between the second extracellular loop of the dopamine D2 receptor and arylpiperazine ligands. *J. Serb. Chem. Soc.* **2012**, *77*, 259–277. [CrossRef]

36. Zhu, J.N.; Liang, L.; Stevens, C.L.K. A CoMFA study of dopamine D2 receptor agonists and X-ray crystal structure of quinelorane dihydrochloride dihydrate, R(-)-apomorphine hydrochloride and R(-)-N-n-propylnorapomorphine hydrochloride. *Struct. Chem.* **2004**, *15*, 553–565. [CrossRef]

37. Modi, G.; Sharma, H.; Kharkar, P.S.; Dutta, A.K. Understanding the Structural Requirements of Hybrid (S)-6-((2-(4-Phenylpiperazin-1-yl)ethyl)(propyl)amino)-5,6,7,8-tetrahydronaphthal en-1-ol and its Analogs as D2/D3 Receptor Ligands: A Three-Dimensional Quantitative Structure-Activity Relationship (3D QSAR) Investigation. *Medchemcomm* **2014**, *5*, 1384–1399.

38. Malo, M.; Brive, L.; Luthman, K.; Svensson, P. Selective pharmacophore models of dopamine D(1) and D(2) full agonists based on extended pharmacophore features. *ChemMedChem* **2010**, *5*, 232–246. [CrossRef]

39. Floresca, Z.C.; Schetz, J.A. Dopamine receptor microdomains involved in molecular recognition and the regulation of drug affinity and function. *J. Recept. Signal Transduct. Res.* **2004**, *24*, 207–239. [CrossRef]

40. Ballesteros, J.A.; Weinstein, H. Integrated methods for the construction of three-dimensional models and computational probing of structure-function relations in G protein-coupled receptors. *Recept. Mol. Biol.* **1995**, *25*, 366–428.

41. Moreira, I.S.S.; Shi, L.; Freyberg, Z.; Ericksen, S.S.; Weinstein, H.; Javitch, J.A. Structural Basis of Dopamine Receptor Activation. In *The Dopamine Receptors*; Neve, K.A., Ed.; Humana Press/Springer: Berlin, Germany, 2010.

42. Salmas, R.E.; Yurtsever, M.; Stein, M.; Durdagi, S. Modeling and protein engineering studies of active and inactive states of human dopamine D2 receptor (D2R) and investigation of drug/receptor interactions. *Mol. Divers.* **2015**, *19*, 321–332. [CrossRef]

43. Bueschbell, B.; Barreto, C.A.V.; Preto, A.J.; Schiedel, A.C.; Moreira, I.S. A Complete Assessment of Dopamine Receptor- Ligand Interactions through Computational Methods. *Molecules* **2019**, *24*, 1196. [CrossRef] [PubMed]

44. Tschammer, N.; Dorfler, M.; Hubner, H.; Gmeiner, P. Engineering a GPCR-ligand pair that simulates the activation of D(2L) by Dopamine. *ACS Chem. Neurosci.* **2010**, *1*, 25–35. [CrossRef] [PubMed]

45. Kling, R.C.; Tschammer, N.; Lanig, H.; Clark, T.; Gmeiner, P. Active-state model of a dopamine D2 receptor-Galphai complex stabilized by aripiprazole-type partial agonists. *PLoS ONE* **2014**, *9*, e100069.

46. Kalani, M.Y.; Vaidehi, N.; Hall, S.E.; Trabanino, R.J.; Freddolino, P.L.; Kalani, M.A.; Floriano, W.B.; Kam, V.W.; Goddard, W.A. The predicted 3D structure of the human D2 dopamine receptor and the binding site and binding affinities for agonists and antagonists. *Proc. Natl. Acad. Sci. USA* **2004**, *101*, 3815–3820. [CrossRef]

47. Holst, B.; Nygaard, R.; Valentin-Hansen, L.; Bach, A.; Engelstoft, M.S.; Petersen, P.S.; Frimurer, T.M.; Schwartz, T.W. A conserved aromatic lock for the tryptophan rotameric switch in TM-VI of seven-transmembrane receptors. *J. Biol. Chem.* **2010**, *285*, 3973–3985. [CrossRef]

48. Degorce, F.; Card, A.; Soh, S.; Trinquet, E.; Knapik, G.P.; Xie, B. HTRF: A technology tailored for drug discovery—A review of theoretical aspects and recent applications. *Curr. Chem. Genom.* **2009**, *3*, 22–32. [CrossRef]

49. Yasi, E.A.; Kruyer, N.S.; Peralta-Yahya, P. Advances in G protein-coupled receptor high-throughput screening. *Curr. Opin. Biotechnol.* **2020**, *64*, 210–217. [CrossRef]

50. Durdagi, S.; Salmas, R.E.; Stein, M.; Yurtsever, M.; Seeman, P. Binding Interactions of Dopamine and Apomorphine in D2High and D2Low States of Human Dopamine D2 Receptor Using Computational and Experimental Techniques. *ACS Chem. Neurosci.* **2015**, *7*, 185–195. [CrossRef]

51. Seeman, P. Antiparkinson therapeutic potencies correlate with their affinities at dopamine D2(High) receptors. *Synapse* **2007**, *61*, 1013–1018. [CrossRef]

52. Tadori, Y.; Forbes, R.A.; McQuade, R.D.; Kikuchi, T. Functional potencies of dopamine agonists and antagonists at human dopamine D(2) and D(3) receptors. *Eur. J. Pharmacol.* **2011**, *666*, 43–52. [CrossRef]

53. Krogsgaard-Larsen, N.; Jensen, A.A.; Schroder, T.J.; Christoffersen, C.T.; Kehler, J. Novel aza-analogous ergoline derived scaffolds as potent serotonin 5-HT(6) and dopamine D(2) receptor ligands. *J. Med. Chem.* **2014**, *57*, 5823–5828. [CrossRef] [PubMed]

54. De Keyser, J.D.B.; De Backer, J.P.; Wilczak, N.; Herroelen, L. Dopamine agonists used in the treatment of Parkinson's disease and their selectivity for the D1, D2, and D3 dopamine receptors in human striatum. *Prog. Neuro-Psychopharmacol. Biol. Psychiat.* **1995**, *19*, 1147–1154. [CrossRef]

55. Mierau, J.; Schneider, F.J.; Ensinger, H.A.; Chio, C.L.; Lajiness, M.E.; Huff, R.M. Pramipexole binding and activation of cloned and expressed dopamine D2, D3 and D4 receptors. *Eur. J. Pharmacol. Mol. Pharmacol.* **1995**, *290*, 29–36. [CrossRef]

56. Heier, R.F.; Dolak, L.A.; Duncan, J.N.; Hyslop, D.K.; Lipton, M.F.; Martin, I.J.; Mauragis, M.A.; Piercey, M.F.; Nichols, N.F.; Schreur, P.J.; et al. Synthesis and biological activities of (R)-5,6-dihydro-N,N-dimethyl-4H-imidazo [4,5,1-ij]quinolin-5-amine and its metabolites. *J. Med. Chem.* **1997**, *40*, 639–646. [CrossRef]

57. Dijkstra, D.; Rodenhuis, N.; Vermeulen, E.S.; Pugsley, T.A.; Wise, L.D.; Wikstrom, H.V. Further characterization of structural requirements for ligands at the dopamine D(2) and D(3) receptor: Exploring the thiophene moiety. *J. Med. Chem.* **2002**, *45*, 3022–3031. [CrossRef]

58. Bonifazi, A.; Yano, H.; Ellenberger, M.P.; Muller, L.; Kumar, V.; Zou, M.F.; Cai, N.S.; Guerrero, A.M.; Woods, A.S.; Shi, L. Novel Bivalent Ligands Based on the Sumanirole Pharmacophore Reveal Dopamine D2 Receptor (D2R) Biased Agonism. *J. Med. Chem.* **2017**, *60*, 2890–2907. [CrossRef] [PubMed]

59. van Wieringen, J.P.; Shalgunov, V.; Janssen, H.M.; Fransen, P.M.; Janssen, A.G.; Michel, M.C.; Booij, J.; Elsinga, P.H. Synthesis and characterization of a novel series of agonist compounds as potential radiopharmaceuticals for imaging dopamine D(2)/(3) receptors in their high-affinity state. *J. Med. Chem.* **2014**, *57*, 391–410. [CrossRef] [PubMed]

60. Kuhhorn, J.; Gotz, A.; Hubner, H.; Thompson, D.; Whistler, J.; Gmeiner, P. Development of a bivalent dopamine D(2) receptor agonist. *J. Med. Chem.* **2011**, *54*, 7911–7919. [CrossRef] [PubMed]

61. Chen, X.; Sassano, M.F.; Zheng, L.; Setola, V.; Chen, M.; Bai, X.; Frye, S.V.; Wetsel, W.C.; Roth, B.L.; Jin, J. Structure-functional selectivity relationship studies of beta-arrestin-biased dopamine D(2) receptor agonists. *J. Med. Chem.* **2012**, *55*, 7141–7153. [CrossRef]

62. Weichert, D.; Banerjee, A.; Hiller, C.; Kling, R.C.; Hubner, H.; Gmeiner, P. Molecular determinants of biased agonism at the dopamine D(2) receptor. *J. Med. Chem.* **2015**, *58*, 2703–2717. [CrossRef]

63. Hiller, C.; Kling, R.C.; Heinemann, F.W.; Meyer, K.; Hubner, H.; Gmeiner, P. Functionally selective dopamine D2/D3 receptor agonists comprising an enyne moiety. *J. Med. Chem.* **2013**, *56*, 5130–5141. [CrossRef] [PubMed]

64. Burris, K.D.; Pacheco, M.A.; Filtz, T.M.; Kung, M.P.; Kung, H.F.; Molinoff, P.B. Lack of discrimination by agonists for D2 and D3 dopamine receptors. *Neuropsychopharmacology* **1995**, *12*, 335–345. [CrossRef]

65. Ghosh, B.; Antonio, T.; Zhen, J.; Kharkar, P.; Reith, M.E.; Dutta, A.K. Development of (S)-N6-(2-(4-(isoquinolin-1-yl)piperazin-1-yl)ethyl)-N6-propyl-4,5,6,7-tetrahydro benzo[d]-thiazole-2,6-diamine and its analogue as a D3 receptor preferring agonist: Potent in vivo activity in Parkinson's disease animal models. *J. Med. Chem.* **2010**, *53*, 1023–1037. [CrossRef]

66. Szabo, M.; Klein Herenbrink, C.; Christopoulos, A.; Lane, J.R.; Capuano, B. Structure-activity relationships of privileged structures lead to the discovery of novel biased ligands at the dopamine D(2) receptor. *J. Med. Chem.* **2014**, *57*, 4924–4939. [CrossRef] [PubMed]

67. Wright, J.L.; Downing, D.M.; Feng, M.R.; Hayes, R.N.; Heffner, T.G.; MacKenzie, R.G.; Meltzer, L.T.; Pugsley, T.A.; Wise, L.D. Identification, characterization and pharmacological profile of three metabolites of (R)-(+)-1,2,3,6-tetrahydro-4-phenyl-1-[(3-phenylcyclohexen-1-yl)methyl]pyridine (CI-1007), a dopamine autoreceptor agonist and potential antipsychotic agent. *J. Med. Chem.* **1995**, *38*, 5007–5014. [CrossRef] [PubMed]

68. Mannel, B.; Dengler, D.; Shonberg, J.; Hubner, H.; Moller, D.; Gmeiner, P. Hydroxy-Substituted Heteroarylpiperazines: Novel Scaffolds for beta-Arrestin-Biased D2R Agonists. *J. Med. Chem.* **2017**, *60*, 4693–4713. [CrossRef]

69. Ghosh, B.A.; Antonio, T.; Reith, M.E.A.; Dutta, A.K. Discovery of 4-(4-(2-((5-Hydroxy-1,2,3,4-tetrahydronaphthalen-2-yl)(propyl)amino)ethyl)piperazin-1-yl)quinolin-8-ol and Its Analogues as Highly Potent Dopamine D2/D3 Agonists and as Iron Chelator: In Vivo Activity Indicates Potential Application in Symptomatic and Neuroprotective Therapy for Parkinson's Disease. *J. Med. Chem.* **2010**, *53*, 2114–2125.

70. Zou, M.F.; Keck, T.M.; Kumar, V.; Donthamsetti, P.; Michino, M.; Burzynski, C.; Schweppe, C.; Bonifazi, A.; Free, R.B.; Sibley, D.R.; et al. Novel Analogues of (R)-5-(Methylamino)-5,6-dihydro-4H-imidazo [4,5,1-ij]quinolin-2(1H)-one (Sumanirole) Provide Clues to Dopamine D2/D3 Receptor Agonist Selectivity. *J. Med. Chem.* **2016**, *59*, 2973–2988. [CrossRef]

71. Linz, S.; Muller, J.; Hubner, H.; Gmeiner, P.; Troschutz, R. Design, synthesis and dopamine D4 receptor binding activities of new N-heteroaromatic 5/6-ring Mannich bases. *Bioorg. Med. Chem.* **2009**, *17*, 4448–4458. [CrossRef]

72. Zhang, J.; Zhang, H.; Cai, W.; Yu, L.; Zhen, X.; Zhang, A. 'Click' D(1) receptor agonists with a 5-HT(1A) receptor pharmacophore producing D(2) receptor activity. *Bioorg. Med. Chem.* **2009**, *17*, 4873–4880. [CrossRef]

73. Cao, Y.; Min, C.; Acharya, S.; Kim, K.M.; Cheon, S.H. Design, synthesis and evaluation of bitopic arylpiperazinephenyl-1,2,4-oxadiazoles as preferential dopamine D3 receptor ligands. *Bioorg. Med. Chem.* **2016**, *24*, 191–200. [CrossRef] [PubMed]

74. Suckling, C.J.; Murphy, J.A.; Khalaf, A.I.; Zhou, S.Z.; Lizos, D.E.; van Nhien, A.N.; Yasumatsu, H.; McVie, A.; Young, L.C.; McCraw, C.; et al. M4 agonists/5HT7 antagonists with potential as antischizophrenic drugs: Serominic compounds. *Bioorg. Med. Chem. Lett.* **2007**, *17*, 2649–2655. [CrossRef] [PubMed]

75. Ali, W.; Wiecek, M.; Lazewska, D.; Kurczab, R.; Jastrzebska-Wiesek, M.; Satala, G.; Kucwaj-Brysz, K.; Lubelska, A.; Gluch-Lutwin, M.; Mordyl, B.; et al. Synthesis and computer-aided SAR studies for derivatives of phenoxyalkyl-1,3,5-triazine as the new potent ligands for serotonin receptors 5-HT6. *Eur. J. Med. Chem.* **2019**, *178*, 740–751. [CrossRef] [PubMed]

76. Löber, S.; Aboul-Fadl, T.; Hübner, H.; Gmeiner, P. Di- and trisubstituted pyrazolo [1,5-a]pyridine derivatives: Synthesis, dopamine receptor binding and ligand efficacy. *Bioorg. Med. Chem. Lett.* **2002**, *12*, 633–636. [CrossRef]

77. Haubmann, C.; Hübner, H.; Gmeiner, P. 2,2-dicyanovinyl as a nonaromatic aryl bioisostere: Synthesis, binding experiments and SAR studies of highly selective dopamine D4 receptor ligands. *Bioorg. Med. Chem. Lett.* **1999**, *9*, 1969–1972. [CrossRef]

78. Cao, J.; Slack, R.D.; Bakare, O.M.; Burzynski, C.; Rais, R.; Slusher, B.S.; Kopajtic, T.; Bonifazi, A.; Ellenberger, M.P.; Yano, H.; et al. Novel and High Affinity 2-[(Diphenylmethyl)sulfinyl]acetamide (Modafinil) Analogues as Atypical Dopamine Transporter Inhibitors. *J. Med. Chem.* **2016**, *59*, 10676–10691. [CrossRef]

79. Kumar, V.; Moritz, A.E.; Keck, T.M.; Bonifazi, A.; Ellenberger, M.P.; Sibley, C.D.; Free, R.B.; Shi, L.; Lane, J.R.; Sibley, D.R.; et al. Synthesis and Pharmacological Characterization of Novel trans-Cyclopropylmethyl-Linked Bivalent Ligands That Exhibit Selectivity and Allosteric Pharmacology at the Dopamine D3 Receptor (D3R). *J. Med. Chem.* **2017**, *60*, 1478–1494. [CrossRef] [PubMed]

80. Reilly, S.W.; Riad, A.A.; Hsieh, C.J.; Sahlholm, K.; Jacome, D.A.; Griffin, S.; Taylor, M.; Weng, C.C.; Xu, K.; Kirschner, N.; et al. Leveraging a Low-Affinity Diazaspiro Orthosteric Fragment to Reduce Dopamine D3 Receptor (D3R) Ligand Promiscuity across Highly Conserved Aminergic G-Protein-Coupled Receptors (GPCRs). *J. Med. Chem.* **2019**, *62*, 5132–5147. [CrossRef]

81. Battiti, F.O.; Cemaj, S.L.; Guerrero, A.M.; Shaik, A.B.; Lam, J.; Rais, R.; Slusher, B.S.; Deschamps, J.R.; Imler, G.H.; Newman, A.H.; et al. The Significance of Chirality in Drug Design and Synthesis of Bitopic Ligands as D3 Receptor (D3R) Selective Agonists. *J. Med. Chem.* **2019**, *62*, 6287–6314. [CrossRef]

82. Neumeyer, J.L.; Baindur, N.; Niznik, H.B.; Guan, H.C.; Seeman, P. (+/−)-3-Allyl-6-bromo-7,8-dihydroxy-1-phenyl-2,3,4,5-tetrahydro-1H-3- benzazepin, a new high-affinity D1 dopamine receptor ligand: Synthesis and structure-activity relationship. *J. Med. Chem.* **1991**, *34*, 3366–3371. [CrossRef] [PubMed]

83. Elsner, J.; Boeckler, F.; Heinemann, F.W.; Hubner, H.; Gmeiner, P. Pharmacophore-guided drug discovery investigations leading to bioactive 5-aminotetrahydropyrazolopyridines. Implications for the binding mode of heterocyclic dopamine D3 receptor agonists. *J. Med. Chem.* **2005**, *48*, 5771–5779. [CrossRef] [PubMed]

84. Enguehard-Gueiffier, C.; Hubner, H.; El Hakmaoui, A.; Allouchi, H.; Gmeiner, P.; Argiolas, A.; Melis, M.R.; Gueiffier, A. 2-[(4-phenylpiperazin-1-yl)methyl]imidazo(di)azines as selective D4-ligands. Induction of penile erection by 2-[4-(2-methoxyphenyl)piperazin-1-ylmethyl]imidazo [1,2-a]pyridine (PIP3EA), a potent and selective D4 partial agonist. *J. Med. Chem.* **2006**, *49*, 3938–3947. [CrossRef] [PubMed]

85. Bollinger, S.; Hubner, H.; Heinemann, F.W.; Meyer, K.; Gmeiner, P. Novel pyridylmethylamines as highly selective 5-HT(1A) superagonists. *J. Med. Chem.* **2010**, *53*, 7167–7179. [CrossRef]

86. Tschammer, N.; Elsner, J.; Goetz, A.; Ehrlich, K.; Schuster, S.; Ruberg, M.; Kuhhorn, J.; Thompson, D.; Whistler, J.; Hubner, H.; et al. Highly potent 5-aminotetrahydropyrazolopyridines: Enantioselective dopamine D3 receptor binding, functional selectivity, and analysis of receptor-ligand interactions. *J. Med. Chem.* **2011**, *54*, 2477–2491. [CrossRef] [PubMed]

87. Prante, O.; Tietze, R.; Hocke, C.; Lober, S.; Hubner, H.; Kuwert, T.; Gmeiner, P. Synthesis, radiofluorination, and in vitro evaluation of pyrazolo [1,5-a]pyridine-based dopamine D4 receptor ligands: Discovery of an inverse agonist radioligand for PET. *J. Med. Chem.* **2008**, *51*, 1800–1810. [CrossRef] [PubMed]

88. Dorfler, M.; Tschammer, N.; Hamperl, K.; Hubner, H.; Gmeiner, P. Novel D3 selective dopaminergics incorporating enyne units as nonaromatic catechol bioisosteres: Synthesis, bioactivity, and mutagenesis studies. *J. Med. Chem.* **2008**, *51*, 6829–6838. [CrossRef]

89. Colabufo, N.A.; Berardi, F.; Perrone, R.; Rapposelli, S.; Digiacomo, M.; Vanni, M.; Balsamo, A. 2-[(3-Methoxyphenylethyl)phenoxy]-based ABCB1 inhibitors: Effect of different basic side-chains on their biological properties. *J. Med. Chem.* **2008**, *51*, 7602–7613. [CrossRef]

90. Berry, C.B.; Bubser, M.; Jones, C.K.; Hayes, J.P.; Wepy, J.A.; Locuson, C.W.; Daniels, J.S.; Lindsley, C.W.; Hopkins, C.R. Discovery and Characterization of ML398, a Potent and Selective Antagonist of the D4 Receptor with in Vivo Activity. *ACS Med. Chem. Lett.* **2014**, *5*, 1060–1064. [CrossRef]

91. Keck, T.M.; Free, R.B.; Day, M.M.; Brown, S.L.; Maddaluna, M.S.; Fountain, G.; Cooper, C.; Fallon, B.; Holmes, M.; Stang, C.T. Dopamine D4 Receptor-Selective Compounds Reveal Structure-Activity Relationships that Engender Agonist Efficacy. *J. Med. Chem.* **2019**, *62*, 3722–3740. [CrossRef]

92. Reilly, S.W.; Griffin, S.; Taylor, M.; Sahlholm, K.; Weng, C.C.; Xu, K.; Jacome, D.A.; Luedtke, R.R.; Mach, R.H. Highly Selective Dopamine D3 Receptor Antagonists with Arylated Diazaspiro Alkane Cores. *J. Med. Chem.* **2017**, *60*, 9905–9910. [CrossRef]

93. Mysinger, M.M.; Carchia, M.; Irwin, J.J.; Shoichet, B.K. Directory of useful decoys, enhanced (DUD-E): Better ligands and decoys for better benchmarking. *J. Med. Chem.* **2012**, *55*, 6582–6594. [CrossRef] [PubMed]

94. Wolber, G.; Langer, T. LigandScout: 3-D pharmacophores derived from protein-bound ligands and their use as virtual screening filters. *J. Chem. Inf. Model.* **2005**, *45*, 160–169. [CrossRef] [PubMed]

95. BIOVIA. *Dassault Systèmes, BIOVIA Discovery Studio, Release 2018*; Dassault Systems: San Diego, CA, USA, 2018.

96. Temml, V.; Kaserer, T.; Kutil, Z.; Landa, P.; Vanek, T.; Schuster, D. Pharmacophore modeling for COX-1 and -2 inhibitors with LigandScout in comparison to Discovery Studio. *Fut. Med. Chem.* **2014**, *6*, 1869–1881. [CrossRef] [PubMed]

97. Vuorinen, A.; Schuster, D. Methods for generating and applying pharmacophore models as virtual screening filters and for bioactivity profiling. *Methods* **2015**, *71*, 113–134. [CrossRef] [PubMed]

98. Lipinski, C.A.; Lombardo, F.; Dominy, B.W.; Feeney, P.J. Experimental and computational approaches to estimate solubility and permeability in drug discovery and development settings. *Adv. Drug Deliv. Rev.* **2001**, *46*, 3–26. [CrossRef]

99. Baell, J.B.; Holloway, G.A. New substructure filters for removal of pan assay interference compounds (PAINS) from screening libraries and for their exclusion in bioassays. *J. Med. Chem.* **2010**, *53*, 2719–2740. [CrossRef]

100. Tanimoto, T.T. *An Elementary Mathematical Theory of Classification and Prediction*; International Business Machines Corporation: Armonk, NY, USA, 1958.

101. Vazquez, J.; Lopez, M.; Gibert, E.; Herrero, E.; Luque, F.J. Merging Ligand-Based and Structure-Based Methods in Drug Discovery: An Overview of Combined Virtual Screening Approaches. *Molecules* **2020**, *25*, 4723. [CrossRef]

102. Smith, J.L.; Stein, D.A.; Shum, D.; Fischer, M.A.; Radu, C.; Bhinder, B.; Djaballah, H.; Nelson, J.A.; Fruh, K.; Hirsch, A.J. Inhibition of dengue virus replication by a class of small-molecule compounds that antagonize dopamine receptor d4 and downstream mitogen-activated protein kinase signaling. *J. Virol.* **2014**, *88*, 5533–5542. [CrossRef]

103. Campiani, G.; Nacci, V.; Bechelli, S.; Ciani, S.M.; Garofalo, A.; Fiorini, I.; Wikstrom, H.; de Boer, P.; Liao, Y.; Tepper, P.G.; et al. New antipsychotic agents with serotonin and dopamine antagonist properties based on a pyrrolo [2,1-b][1,3]benzothiazepine structure. *J. Med. Chem.* **1998**, *41*, 3763–3772. [CrossRef]

104. Naporra, F.; Gobleder, S.; Wittmann, H.J.; Spindler, J.; Bodensteiner, M.; Bernhardt, G.; Hubner, H.; Gmeiner, P.; Elz, S.; Strasser, A. Dibenzo[b,f][1,4]oxazepines and dibenzo[b,e]oxepines: Influence of the chlorine substitution pattern on the pharmacology at the H1R, H4R, 5-HT2AR and other selected GPCRs. *Pharmacol. Res.* **2016**, *113*, 610–625. [CrossRef]

105. Ginex, T.; Munoz-Muriedas, J.; Herrero, E.; Gibert, E.; Cozzini, P.; Luque, F.J. Development and validation of hydrophobic molecular fields derived from the quantum mechanical IEF/PCM-MST solvation models in 3D-QSAR. *J. Comput. Chem.* **2016**, *37*, 1147–1162. [CrossRef] [PubMed]

106. Meyer, J.M.; Ejendal, K.F.; Avramova, L.V.; Garland-Kuntz, E.E.; Giraldo-Calderon, G.I.; Brust, T.F.; Watts, V.J.; Hill, C.A. A "genome-to-lead" approach for insecticide discovery: Pharmacological characterization and screening of Aedes aegypti D(1)-like dopamine receptors. *PLoS Negl. Trop. Dis.* **2012**, *6*, e1478. [CrossRef] [PubMed]

107. Bogeso, K.P.; Liljefors, T.; Arnt, J.; Hyttel, J.; Pedersen, H. Octoclothepin enantiomers. A reinvestigation of their biochemical and pharmacological activity in relation to a new receptor-interaction model for dopamine D-2 receptor antagonists. *J. Med. Chem.* **1991**, *34*, 2023–2030. [CrossRef]

108. Staron, J.; Kurczab, R.; Warszycki, D.; Satala, G.; Krawczyk, M.; Bugno, R.; Lenda, T.; Popik, P.; Hogendorf, A.S.; Hogendorf, A.; et al. Virtual screening-driven discovery of dual 5-HT6/5-HT2A receptor ligands with pro-cognitive properties. *Eur. J. Med. Chem.* **2020**, *185*, 111857. [CrossRef] [PubMed]

109. Perrone, R.; Berardi, F.; Colabufo, N.A.; Leopoldo, M.; Tortorella, V. A structure-affinity relationship study on derivatives of N-[2-[4-(4-Chlorophenyl)piperazin-1-yl]ethyl]-3-methoxybenzamide, a high-affinity and selective D(4) receptor ligand. *J. Med. Chem.* **2000**, *43*, 270–277. [CrossRef] [PubMed]

110. Peprah, K.; Zhu, X.Y.; Eyunni, S.V.; Setola, V.; Roth, B.L.; Ablordeppey, S.Y. Multi-receptor drug design: Haloperidol as a scaffold for the design and synthesis of atypical antipsychotic agents. *Bioorg. Med. Chem.* **2012**, *20*, 1291–1297. [CrossRef] [PubMed]

111. Schoemaker, H.; Claustre, Y.; Fage, D.; Rouquier, L.; Chergui, K.; Curet, O.; Oblin, A.; Gonon, F.; Carter, C.; Benavides, J.; et al. Neurochemical characteristics of amisulpride, an atypical dopamine D2/D3 receptor antagonist with both presynaptic and limbic selectivity. *J. Pharmacol. Exp. Ther.* **1997**, *280*, 83–97.

112. Poli, G.; Seidel, T.; Langer, T. Conformational Sampling of Small Molecules With iCon: Performance Assessment in Comparison With OMEGA. *Front. Chem.* **2018**, *6*, 229. [CrossRef]

113. Kaserer, T.; Beck, K.R.; Akram, M.; Odermatt, A.; Schuster, D. Pharmacophore Models and Pharmacophore-Based Virtual Screening: Concepts and Applications Exemplified on Hydroxysteroid Dehydrogenases. *Molecules* **2015**, *20*, 22799–22832. [CrossRef]

114. Sander, T.; Freyss, J.; von Korff, M.; Rufener, C. DataWarrior: An open-source program for chemistry aware data visualization and analysis. *J. Chem. Inf. Model.* **2015**, *55*, 460–473. [CrossRef]

115. Glen, R.C.; Bender, A.; Arnby, C.H.; Carlsson, L.; Boyer, S.; Smith, J. Circular fingerprints: Flexible molecular descriptors with applications from physical chemistry to ADME (vol 9, pg 199, 2006). *Idrugs* **2006**, *9*, 311.

116. Rogers, D.; Hahn, M. Extended-connectivity fingerprints. *J. Chem. Inf. Model.* **2010**, *50*, 742–754. [CrossRef]